Implementation of Electrochemical Impedance Spectroscopy on the Mobile Phone

By Changlong Zou

A thesis

submitted in partial fulfillment of the

requirements for the degree of

Master of Science

University of Washington

2015

Committee:

Daniel T. Schwartz

Eric M.Stuve

Qiuming Yu

Program Authorized to Offer Degree:

Chemical Engineering

University of Washington

Abstract

Implementation of Electrochemical Impedance Spectroscopy on the Mobile Phone

Changlong Zou

Chair of the Supervisory Committee:
Boeing-Sutter Professor Daniel T. Schwartz
Chemical Engineering

Lithium-ion batteries are widely used in portable devices, household electronics, and transportation vehicles. Accurately estimating the state of charge (SOC), state of health (SOH), and remaining usable lifetime (RUL) of Li-ion batteries is increasingly important. New diagnostic method are needed to improve battery management and performance. Here we review electrochemical impedance spectroscopy (EIS) based SOC and SOH estimation methods. We then introduce a new method to do EIS on portable devices. We show that screen brightness modulations can be used to produce a modulated current at the battery. The modulated current induces a modulated voltage signal. Fast Fourier Transforms (FFTs) of the current and voltage signals are used to determine the battery impedance at the modulation frequency. An Android application is used to control the screen modulation and make the current and voltage

measurements on the phone. The prototype EIS application is demonstrated as a potentially valuable new characterization tool for on-device battery diagnostics.

Table of Contents

1. Introduction

Worldwide awareness of environmental pollution from fossil energy encourages the development of clean energy. Accelerated by the tragedy of the Fukushima nuclear power plant in 2011, the conversion to clean energy sources make batteries an increasingly attractive energy storage system[1] [2]. Among different batteries, Lithium-ion (Li-ion) cells have attracted the most attention due to their many advantages: high cell voltage, high power/energy density, low pollution, low self-discharge rate, and high cycle life [2] [3]. Li-ion is increasingly popular in portable electronics, automotive and green energies industries[4] [5]. However, the complex physical and chemical processes inside a battery during operation can lead to problems, e.g. aging, accelerated degradation, and catastrophic failure. It is difficult to detect and avoid these processes. For example, the Li-ion battery system in Boeing's 787 Dreamliner aircraft caught fire in 2013 and grounded the fleet for months [6]. Hence, improved on-board battery characterization coupled to a sophisticated battery management system (BMS) is essential for growing the use and performance of Li-ion battery systems. An ideal diagnostic tool will monitor the state of a battery, predict the failure of batteries and provide a signal that might be usable for specific controlling actions, e.g. during charging and discharging [7] [8]. State of charge (SOC) and state of health (SOH) are two common indicators used to describe the state of batteries. Briefly, SOC tells the amount of energy stored in battery. SOH tells about the aging and degradation effects inside batteries[9].

In the literature, there are many different approaches being used to determine SOC and SOH. Each approach has its own strategy and advantages. However, accurate estimation of SOC and SOH is complex and difficult to implement, due to the limitation of battery models and parametric uncertainties [10]. As one of these different choices, electrochemical impedance spectroscopy (EIS) is considered a powerful experimental method for investigating the operational mechanism, aging mechanism and thermal degradation inside the battery [11]. However, EIS is normally implemented as a laboratory analytical method, not as an on-board test. This thesis will review details about EIS and its application to determining SOC and SOH, and show its potential for implementing on a device. A prototype Android App is designed to illustrate this idea and discussion is focused on further improvements.

1.1 Electrochemical Impedance Spectroscopy

EIS is a perturbative method that characterizes the dynamics of an electrochemical process. It is used as a tool to unravel complex non-linear processes in many material systems and applications. e.g., corrosion, plating, batteries, fuel cells, etc.[12].When evaluating a Li-ion battery, EIS can provide a non-destructive analysis of electrode/electrolyte interfaces, intercalation kinetics, lithium ion transport, aging and thermal degradation [13] [14] [15] [16]. The kernel of EIS is to measure electrochemical impedance at different frequencies. Electrochemical impedance is usually measured by applying an AC potential to an electrochemical cell and then measuring the current through the cell, or vice versa, modulating current and measuring voltage.[17] For example, when superimposing a periodic potential perturbation to a normal operating voltage, the battery current will oscillate around the operating point. The current response can be collected and the frequency response analyzed as a Fourier series[18] [19]. However, the processes within Li-ion batteries are strongly nonlinear, so the perturbation signal needs to be small enough to ensure the cell's response follows pseudo-linear behavior. In a linear (or pseudo-linear) system, a sinusoidal perturbation input will produce a sinusoidal output response at the same frequency but shifted in amplitude and phase [17] [18] [19].

For potentiodynamic modulations, a sinusoidal voltage perturbation is superimposed on the mean voltage V_0. The modulated potential V can be expressed in both trigonometric form and complex form:

$$V = V_0 + \Delta V * sin(\omega t) \tag{1}$$

$$V = V_0 + \Delta V * e^{j\omega t} \tag{2}$$

Where, ΔV is the amplitude of the sinusoidal perturbation voltage; ω is the radial frequency that equals to $2\pi f$; j is the square root of -1. According to the pseudo-linear assumption, the corresponding current response should be expressed as:

$$I = I_0 + \Delta I * sin(\omega t + \varphi) \tag{3}$$

$$I = I_0 + \Delta I * e^{j(\omega t - \varphi)} \tag{4}$$

Where, I is the transient current; I_0 is the mean operating current; ΔI is the amplitude of current perturbation induced by the voltage perturbation; φ is the phase shift between the current perturbation and voltage perturbation. Under the pseudo-linear assumption, impedance can be calculated analogously to Ohm's Law using voltage/current perturbation values [17] [18] [19]:

$$Z = \frac{\tilde{V}}{\tilde{I}} = \frac{\Delta V * sin(\omega t)}{\Delta I * sin(\omega t + \varphi)} \tag{5}$$

$$Z = Z_{re} + Z_{im} = \frac{\tilde{V}}{\tilde{I}} = \frac{\Delta V * e^{j\omega t}}{\Delta I * e^{j(\omega t - \varphi)}} = \frac{\Delta V}{\Delta I} * e^{j\varphi} = \frac{\Delta V}{\Delta I} * (cos(\varphi) + j * sin(\varphi))(6)$$

The two expressions of impedance are consistent but in different forms. Considering both expressions, it indicates that impedance depends on the frequency and magnitude of voltage/current perturbation and the phase shift between voltage/current perturbations.

For galvanodynamic modulations, the general scenario is analogous to potentiodynamic modulation except that current perturbation is controlled instead of voltage perturbation. The expression of impedance of galvanostatic model is equivalent to equation (6). As a consequence of the above calculations at different perturbing frequencies, varying from low to high, a series of generalized impedances will form an impedance spectrum which depends on chemical and physical processes, material properties, microstructure, and surface reactions as well as different operating conditions such as temperature[18] [19] [20].

1.2 Impedance Spectrum

Impedance spectra normally are presented in two ways: Nyquist Plots and Bode Plots. On Nyquist plots, the real part of impedance Z is plotted on the x-axis and the (negative) imaginary part is plotted on the y-axis of a chart. Each point on the Nyquist

Plot is the impedance at a single frequency. Figure 1 is an example of a Nyquist plot that has a capacitive loop. The frequency increases as one travels counter-clockwise along the loop. The impedance at any point also can be represented as a vector (arrow) of length $|Z|$. $|Z|$ is the modulus of Z which can be calculated from:

$$|Z| = \frac{\Delta V}{\Delta I} \ or = \sqrt{Re(Z)^2 + Im(Z)^2} \tag{7}$$

The angle between this vector and the x-axis is phase angl$e$ $\varphi = arg\,Z$ which equals the phase shift. Since Nyquist plots convey key characteristics of the electrochemical system, it is more frequently used in experiments.

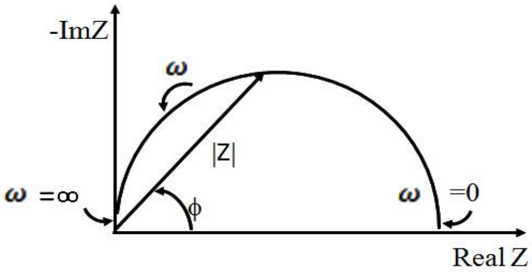

Figure 1. Example of Nyquist plot [17]

Unlike Nyquist plots, a Bode plot requires two separate graphs to present the impedance. One is graph plots the modulus of Z and the other plots the phase shift of Z against the log frequency on the x-axis. Figure 2 is an example of Bode plot.

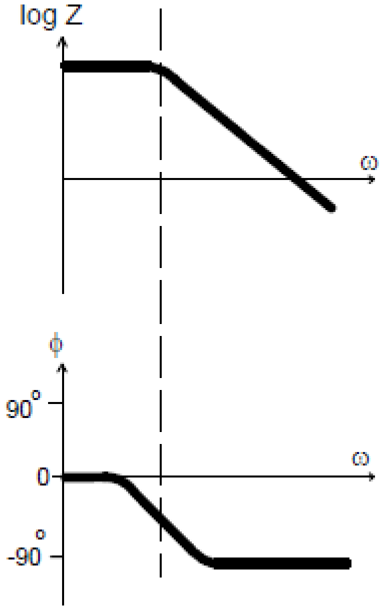

Figure 2. Example of bode plot [17]

A Bode plot lacks clear information about the behavior of the electrochemical device, but it consists of clearer information about frequencies that dictate the key time-scales of the system [20].

1.3 Measurement techniques

Most EIS investigations are performed with a frequency response analyzer in conjunction with a precision electrochemical instrument. Normally, the perturbation signals are periodic signals e.g. sinusoid waves. But there are some cases using white noise or background noise as perturbation signals[21] [22]. The accuracy of measurement depends on the target system and measuring condition. For example, when measuring the low impedances of high capacity Li-ion battery, the connecting resistance between leads or connectors are significant compared to the battery impedance[23]. This errors can be minimized by improving measurement with three or four leads to eliminate errors. In addition, errors may also be observed at high frequency impedance measurement, if the current-measuring resistor of the electrochemical interface is small ($< 0.1\Omega$)[24].

1.4 Application of EIS to Battery Equivalent Circuit Models

In the literature, equivalent circuit models (ECM) are introduced to describe and simulate the various transport and kinetic processes in the electrochemical system. The main equivalent circuit elements are introduced below.

Electrical double-layer capacitance. $\boldsymbol{C_{dl}}$

Electrical double-layer capacitance describes the capacitive behavior that is caused by a charged region adjacent to an electrode due to the separation of ions and surface charges at the interface. Both electrodes in the battery contribute to this capacitive behavior [18][25]. The capacitance depends on the electrode voltage [26].

Charge-transfer resistance. $\boldsymbol{R_{ct}}$

A resistance in parallel with C_{dl} is used to model the charge-transfer process that happens at each electrode during intercalation. Theoretically, the resistance can be derived from Butler-Volmer equation[27]. For a charge-transfer process:

$$I_r = A * i_0 * (\exp\left(\frac{\alpha_a * F}{R_{gas} * T} * \Delta U_r\right) - \exp\left(-\frac{\alpha_c * F}{R_{gas} * T} * \Delta U_r\right) \qquad (8)$$

Where, the two exponential terms describes the reversible redox reaction rates for cathodic and anodic deviations from equilibrium; A is the active surface coefficient; ΔU_r is the voltage deviation from equilibrium; i_0 is the exchange current density; T is the operating temperature; R_{gas} is the universal gas constant; F is the Faraday constant; α_a and α_c are coefficients related to the symmetry of the reaction between charging and discharging [27]. In analogy to Ohm's Law, the charge-transfer resistance can be expressed as a function of I_r because ΔU_r can be described as a function of I_r.

$$R(I_r) = \frac{\Delta U_r}{I_r} \tag{9}$$

Obviously, the relation between charge-transfer resistance and current is nonlinear.

Diffusion &Warburg Element. Z_w

Because of the effect of diffusion, there is mass transport of ions within the battery. Since, the movement of ions within electrodes and electrolyte is driven by concentration gradients, the effect of diffusion can be described by Fick's Law [27]. A Warburg element is introduced to model the diffusion process in electrochemistry [28]. Generally, it performs as a capacitive circuit similar to double-layer effect combined with charge-transfer process. But, there is more than one order of magnitude of different between the time-constants of these two processes, which makes the effect of diffusion, Warburg element become significant at very low frequency of perturbation [28][29]. For a siple diffusion process, the Warburg element can be expressed as:

$$Z_w = \frac{RT}{cn^2F^2A_e} * \frac{1}{\sqrt{j\omega D}} \tag{10}$$

Where, R is the universal gas constant; T is the temperature; c is the molarity; n is the charger number; F is the Faraday constant; A_e stands for the active surface and D is the diffusion coefficient. This expression is valid for a moderate range of frequencies. When the frequency becomes too low, the expression of Warburg impedance will be different depending on the boundary conditions [28] [29]

Ohmic Resistance. R_0

R_0 represents the sum of all pure ohmic resistances in the battery and measurement device. Generally, it includes the resistance of electrolyte, electrode substrate metal, electrode leads, terminals and contacting resistances[30].

Inductance. L

It represents the inductive impedance behavior observed at high frequency in the battery. According to[31], the inductance is due to the porosity of the electrodes and the fact that cell types are formed into compact cylinders. Since, the inductive behavior become significant only at high frequency range, it can be neglected for measurement at low-medium frequency range in order to simplify the ECM.

Combine these elements, an ECM describing the full battery cell is introduced in Figure 3. This simple ECM is widely accepted as a basic descriptor of the linear impedance [27] [**Error! Bookmark not defined.**] [28] [29] [30] [31].

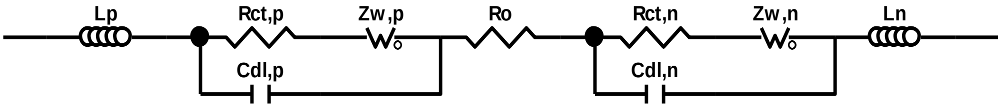

Figure 3. ECM of a full battery cell

The subscripts p and n stand for positive and negative electrodes respectively in Figure 3.

1.5 Relationship between Nyquist Plots and the ECM.

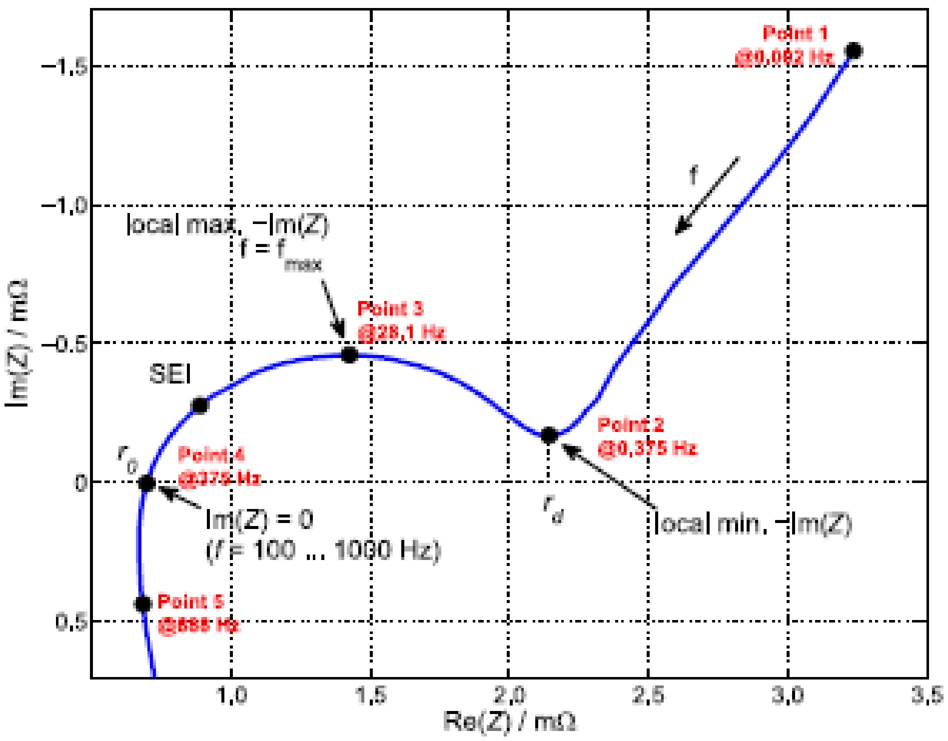

Figure 4. Nyquist plot of the complex impedance of a Kokam 40Ah lithium-ion battery with NMC cathode at 10℃ and 90%SOC. [27]

A Nyquist plot of a Li-ion battery from [27] is used here for illustration.

The region between point 1 and point 2 is the low frequency range describes the Warburg impedance. The shape of the impedance indicates that the boundary condition for this battery is quasi-infinite diffusion length [27].

The semicircle between point 2 and point 4 represents the charge-transfer reactions combined with capacitive behaviors from both cathode and anode. Since the total impedance of battery can be expressed:

$$Z = \frac{1}{\frac{1}{R_{ct}} + j\omega C_{dl}} + R_0 \tag{11}$$

At point 2, the resistance of C_{dl} becomes very large due to the low frequency: $\frac{1}{j\omega C_{dl}} \rightarrow \infty$. Hence, impedance presents purely resistive behavior.

$$Z = r_d \approx R_{ct} + R_0 \tag{12}$$

Where, r_d is the real part of impedance at point 2.

In contrast, at point 4, the resistance of C_{dl} becomes very small due the high frequency: $\frac{1}{j\omega C_{dl}} \rightarrow 0$. Hence, impedance also presents purely resistive behavior, but:

$$Z = r_0 = R_0 \tag{13}$$

Where, r_0 is the real part of impedance at point 4 when imaginary part of impedance is zero.

In general, both ohmic resistance and charge-transfer resistance can be calculated from point 2 and point 4 by: $R_0 = r_0$ and $R_{ct} \approx r_d - r_0$.

Point 3 is the local maximum imaginary part of impedance. Assuming the battery behavior in this frequency range as an ideal RC circuit, then the magnitudes of imaginary and real part of impedance at point 3 should be equal. The double-layer capacitance can be approximated as:

$$\frac{1}{2R_{ct}} = \omega C_{dl} = 2\pi f_{max} C_{dl} \tag{14}$$

$$C_{dl} = \frac{1}{2\pi f_{max} R_{ct}} \tag{15}$$

Where, f_{max} is the frequency at point 3.

At point 5, the imaginary part of impedance is positive, which is an inductive behavior. At point 4, the imaginary part of impedance is zero. It indicates the balance of capacitive and inductive at that frequency. Hence, if frequency becomes higher, the effect of inductance will be visible on the plot, and the impedance will increase with frequency.

In Figure 4, solid electrolyte interface (SEI) is indicated on the semicircle. Theoretically, the effect of SEI will form a smaller semicircle during aging. But for this investigated cell, the SEI semicircle is so small and merged into the big semicircle[32]. Theoretically, the impedances of two electrodes are different so that each electrode will form a semicircle separately, which is proved by the measurement of the EV-30 battery in this thesis and other papers [1] [18] [32][33].

1.6 EIS based SOC, SOH, and RUL determination

Since EIS has the ability to measure electrical parameters used to model molecularly-related processes involved in batteries, it has been widely researched to extract parameters that related to SOC, SOH and RUL in many papers [30] [32] [34] [35] [36] [37] [38] [39] [40] [41].

SOC Determination

In general, the SOC of a battery is defined as the ratio of current capacity to the nominal capacity. The nominal capacity is the maximum amount of charge (Q_n) that can be stored in the battery, which varies from manufacturers and designs. Hence, the SOC can be expressed as the estimated amount of charge in the battery at time, *t*, divided by the maximum charge:

$$SOC(t) = \frac{Q(t)}{Q_n} \tag{16}$$

Investigating the dependence of electrical parameters on SOC is done in a similar manner in many papers. EIS measurements applied to the same battery with different SOCs (at same temperature), are then used as single or pairs of parameters to correlate their dependences on SOC. Maintaining the operating temperatures the same for different measurements is critical, since the impedance of batteries depend on temperature significantly [33] [34].

The fact that the semicircle at medium to low frequency range on the Nyquist plot is significantly varying with SOC is observed in many papers [9] [10] [19] [30] [31] [32] [34] [35] [36] [37]. In [19], it shows that the ohmic resistance of the nickel-cadmium battery has an excellent linear correlation with SOC, but the difference between the Ohmic resistances at 100% and 0% of SOC is less than 7%. The charge-transfer resistance shows a negative exponential correlation with SOC and a maximum of 60% variation. A correlation between charge-transfer resistance of positive electrodes and SOC is observed in lithium ion batteries [32] [33] [38]. Around 40% - 80% variation of charge-transfer resistances is observed from 0% to 100% SOC, indicating a strong dependence. The magnitude of variation also shows dependence on charge/discharge rate and operating temperature. The ohmic resistances measured are considered constant for different SOCs since small variations (<10%) are observed. In [33], a non-monotonic correlation between ΔR_{ct} and SOC for lithium ion battery is seen, where ΔR_{ct} is the difference between charge-transfer resistances at the positive electrode for charging and discharging. From 100% to 50% of SOC, ΔR_{ct} is positive and proportional to the SOC. But, from 50% to 25% of SOC, ΔR_{ct} is negative and inversely proportional to the SOC. This correlation is partially explained by analysis of lithium-ion concentration at electrode/electrolyte interface.

The dependence of double-layer capacitance on SOC is investigated in [38]. Some correlations between double-layer capacitance and SOC are observed with small variations. In contrast to investigating the SOC dependence directly with the time consuming low frequency range measurements, H. Blanke [36] proposes impedance correlation with SOC at high frequencies. A transition frequency is defined as point 4 on Figure 4 where the imaginary component is zero. Since, the inductive impedance is almost constant at various SOCs, the capacitive impedance at high frequency range is the main SOC related element. Hence, the transition frequency will change with SOC. A negative exponential dependence of transition frequency on SOC is obtained from measurements.

The dependence of the RC time constant τ on SOC is investigated in [38] and gives a negative exponential relationship. The time constant τ is defined as:

$$\tau = R_{ct} * C_{dl} = \frac{1}{2\pi f_{max}} \tag{17}$$

Essentially, the dependence of τ on SOC is the dependence of R_{ct} and C_{dl} on SOC. Since, C_{dl} can be considered as constant for most cases, it can be predicted that τ behaves like R_{ct} dependency on SOC.

In conclusion, the charge-transfer resistance and its related parameters have the most direct and detectable correlation with SOC and can be easily identified on a Nyqusit plot.

SOH and RUL determination

SOH reflects the aging process of the battery cell [39]. The aging mechanism consists of loss of recyclable lithium, internal resistance increasing due to the growth of solid-electrolyte interface (SEI), and loss of active materials due to dissolution into electrolyte or electrical isolation caused by cracking of the electrode conductive matrix [42] [43] [44]. Practically, direct inspection of electrodes structure, materials concentration and etc. are impossible in a sealed battery. SOH determinations are usually based on parameters that can be measured with non-destructive tests. In some literature, SOH is defined as the remaining capacity of the battery or remaining useful life (RUL) which directly tells how long the battery can operate. However, the only reliable method to measure the remaining capacity is to discharge the battery [19].

Instead of remaining capacity, SOH can also be defined as the increase in battery resistance [39]. EIS can be used to track resistance changes [36] [39]. In [19] [35] [36]

[39] the ohmic resistance increases with aging, shifting the impedance spectrum to the right on a Nyqusit plot. The increase may due to the increase of resistance between current collector and active mass at positive electrode, combined with the effect of increasing SEI thickness. In [39] the charge-transfer resistance also shows a significant increase in aged batteries. A decrease of the double-layer capacitance is observed during aging in long term tracking. Furthermore, B.Saha [41] proposes an inverse proportionality between the RUL and the sum of ohmic and charge-transfer resistance. Thus, good prediction of RUL can be obtained based on EIS results.

Implementation on mobile devices

For large battery packs, SOC and SOH estimation are critical function for stable and safe operation [3]. Estimation based on empirical models[45], linearized models of the PDAE system [46], single particle model[47], open circuit voltage monitoring and ampere hour counting or coulomb counting [9] are widely used in different battery management systems (BMSs). For example, the Tesla Roadster BMS is using calculated ampere hour counting method to estimate SOC[48]. EIS based battery SOC observer [3] and SOH predictor [35] are introduced in recent years. But few EIS based BMS diagnostics are found in industry due to the complex analytical instruments that are normally associated with EIS.

SOC estimation on portable devices usually depends on the open circuit voltage (OCV) and coulomb counting method [3]. The relationship between OCV and SOC is not linear and differs for different lithium ion batteries[49] [50]. It is difficult to get accurate estimation of SOC without measurement of the OCV-SOC dependency[51]. The coulomb counting method measures the discharging current of the battery and integrates over a period of time to estimate SOC [52] as:

$$SOC(t) = SOC(t-1) + \frac{I(t)}{Q_n} * \Delta t \tag{18}$$

But the accuracy of this method is strongly affected by temperature, aging effect, discharge current and cycle life [52]. Apps like Carat [53] and Batteryscore[54] are used on mobile phones to help in SOC, SOH and RUL estimation. A long term continuous recording of voltage and current data or data from a cloud database is used as reference to estimate SOC, SOH and RUL with instantaneous voltage or current readings. No application of EIS based estimation is found for mobile phones. However, many chipsets installed in cell phones are powerful. For example, the DS2760 Smart Battery Monitor chip produced by Maxim can achieve a sampling frequency up to 1500Hz on voltage and current with 0.625mA current resolution and 5mV voltage resolution[55]. Furthermore, current or voltage perturbation can be excited through various methods, e.g., the charging current from a charger, varying discharging current by adjustment of volume or frequency of audio, and color or brightness of display screen. The essential requirements for EIS can be fulfilled by the function of mobile phones without additional analytical instruments.

The next section illustrates procedures to achieve implementation of EIS on a mobile phone.

2. Analysis

2.1 Battery ECM

Key parameters of SOC and SOH estimation are ohmic resistance (R_0) and charge-transfer resistance (R_{ct}), which can be measured by EIS at moderate low to the high frequency range. Hence, the inductive impedance at high frequency and Warburg impedance at low frequency are not needed in the ECM used here.

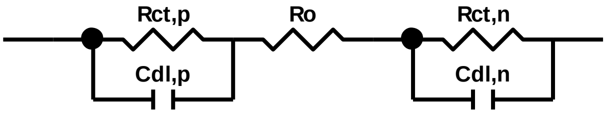

Figure 5. ECM of battery used in the thesis.

In Figure 5, the subscripts p and n denote positive and negative electrode respectively. Hence, the impedance of the battery over intermediate frequencies can be expressed as:

$$Z_{battery} = R_0 + \frac{1}{\frac{1}{R_{ct,p}} + j\omega C_{dl,p}} + \frac{1}{\frac{1}{R_{ct,p}} + j\omega C_{dl,p}} \tag{19}$$

2.2 App Design

The three main current consuming operations on a phone are the screen display (80%), CPU (10%), and system kernel (5%). The usage of CPU and system kernel is difficult to predict and control since it depends on all the background and foreground processing. In contrast, the variation of background color or brightness of the display screen can be controlled easily to excite current perturbations.

Our experimental mobile phone is a Motorola Droid Razr Maxx HD operating with Android OS version 4.1.2. The battery is a Motorola EV-30 3.8V, 2500±30 mAh Lithium ion polymer battery. This phone has a 4.7 inch Super AMOLED capacitive touch screen, which is an idea source for current perturbations. Its Dual-core 1.5 GHz CPU allows it to read and write data fairly fast.

The color and brightness of the display screen are controlled in ARGB format, where A stands for α, the opacity of the screen. All four parameters range between 0-255, where 0 means no contribution and 255 means 100% contribution. In order to minimize the influence from current variation caused by background processes, and minimize the complexity of the App, RGB components are set to 255 which refers to a white screen color, and current perturbation is excited by adjusting the α value in real time to make screen flash periodically.

2.3 Transfer function Relating Screen modulation to Current modulation

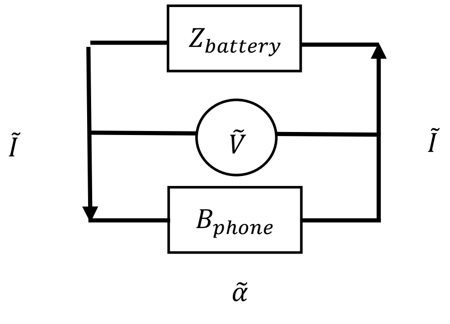

Figure 6. Illustration of the phone and battery system.

Figure 6 is a simple presentation of the phone and battery system. The impedance of battery can be calculated as

$$Z_{battery} = \frac{\widetilde{V}}{\tilde{I}} \tag{20}$$

but it is less clear how the flashing of the screen opacity will be linked to the current oscillation. We call the relationship between screen opacity and current the phone transfer function:

$$B_{phone} = \frac{\widetilde{I}}{\tilde{\alpha}} \tag{21}$$

where, $\tilde{V}$ and $\tilde{I}$ are the voltage and current perturbations at the contacting terminals of the battery respectively; $\tilde{\alpha}$ is the perturbation of opacity of the screen.

Since the phone is an active electrical device, not simply a passive system, it may be a misnomer to call this a transfer function. We need to investigate the nature of B_{phone} and how it depends on perturbation frequency and other factors tied to the phone operation, if we hope to calculate $Z_{battery}$ reliably on the phone. In short, for an accurate measurement of the $Z_{battery}$, the "transfer function" B_{phone} must be well behaved and predictable.

2.4 Pseudo-steady current perturbation

The phone cannot rigorously run in a pure galvanodynamic or potentiodynamic mode for EIS measurement when self-powered. Flashing the screen opacity generates a power fluctuation involving both current and voltage fluctuations simultaneously. For a complex power function:

$$P(\omega) = P_0 + \Delta P_{re}(\omega) * cos(\omega t) + \Delta P_{im}(\omega) * j * sin(\omega t) \tag{22}$$

It also can be expressed in terms of complex current and voltage.

$$P(\omega) = I(\omega) * V(\omega)$$

$$= [I_0 + \Delta I_{re}(\omega) * cos(\omega t) + \Delta I_{im}(\omega) * j * sin(\omega t)] * [V_0 + \Delta V_{re}(\omega) * cos(\omega t) + V_{im}(\omega) * j * sin(\omega t)]$$

$$= I_0 * V_0 + (I_0 * \Delta V_{re} + V_0 * \Delta I_{re}) * cos(\omega t) + j * (I_0 * \Delta V_{im} + V_0 * \Delta I_{im}) * sin(\omega t) + \Delta V_{re} * \Delta I_{re} * cos^2(\omega t) - \Delta V_{im} * \Delta I_{im} * sin^2(\omega t) + j * (\Delta V_{re} * \Delta I_{im} + \Delta V_{im} * \Delta I_{re}) * cos(\omega t) * sin(\omega t)$$

This equation can be segregated into the mean, linear, and nonlinear terms by using trigonometric relationships, to yield the leading order mean power

$$[I_0 * V_0] \qquad (23a)$$

and the linear fluctuations

$$[(I_0 * \Delta V_{re} + V_0 * \Delta I_{re}) * cos(\omega t) + j * (I_0 * \Delta V_{im} + V_0 * \Delta I_{im}) * sin(\omega t)] \qquad (23b)$$

where I_0 and V_0 are mean current and mean voltages, respectively; ΔV_{re} and ΔV_{im} are magnitudes of real and imaginary part of voltage deviation; ΔI_{re} and ΔI_{im} are magnitudes of real and imaginary part of current perturbation; ω is the radial frequency.

The linear fluctuations term is the one consisting of information related to impedance measurement, and can be rewritten as:

$$I_0 V_0 \left[\left(\frac{\Delta V_{re}}{V_0} + \frac{\Delta I_{re}}{I_0}\right) * cos(\omega t) + j * \left(\frac{\Delta V_{im}}{V_0} + \frac{\Delta I_{im}}{I_0}\right) * sin(\omega t)\right] \qquad (24)$$

We will show later that the magnitude of voltage fluctuations is small compared to the mean voltage whereas the magnitude of current fluctuations are nearly comparable to the mean currents. When this is true, power fluctuations on the phone are, to leading order, synonymous with current perturbation. In other words, the power perturbation can be regarded as pseudo-current perturbation.

3. Methods and Procedures

3.1 App Design Procedures

We set the α value varying from 0 to 255 in steps of 10 every 10 second interval. At the same time, we read transient current data from the battery monitor chipset at several user defined frequencies. For this phone, current readings are requested from “sys/class/power_supply/battery/current_now”. Data is saved into a txt file. As initially setting up, current readings from the chipset are assume to be correct. The accuracy of readings will be tested in later experiments.

Extract current readings file from phone, and use Matlab or Excel to calculate the current function on the dependency of α value.

Calculate the α values needed to form a sin/cosine current perturbation. In this thesis, the App is designed to use 32 points to simulate a cosine signal. Hence, 32 solutions will be solved from:

$$I = f(\alpha) \tag{25}$$

$$I = I_o + \Delta I * cos(\omega t) \tag{26}$$

Where I_o is the mean current; ΔI is the designed perturbation amplitude.

For applying EIS on the mobile phone, the App is ordered to change the α values one by one according to above solutions. The frequency of the perturbation is controlled by adjusting the rest time for the App before setting a new α value. At the same time another thread of the App is recording the voltage and current readings from the files locations mentioned above. The Voltage reading file is saved at the location “sys/class/power_supply/battery.voltage_now”. The sampling frequency is controlled by adjusting the rest time for the App before sending a new request to access the locations.

The frequency range of EIS is limited by both current perturbation and data sampling processes. For current perturbation process, the minimum rest time is 7-8 ms corresponding to 33Hz.

3.2 Experiment 1. Validation of the App

A Princeton Applied Research Model 362 Scanning Potentiostat is connected to the phone, and set to run on potentiostat-mode as a power supply at constant 3.9V volts. We run the App on the phone. The frequency of current perturbation ranges starts from 0.125Hz and reaches a high value of 1.25Hz, 2.5Hz. and 4Hz when we use a corresponding 16, 8, or 4 sampling points per current perturbation cycle, respectively. The voltage and current are measured by the potentiostat at the same time. LabView is used as interface on PC to record the data through a NI CB-50LP Digital I/O DAQ board at a constant 32 points per current perturbation cycle sampling rate.

Data collected from the App is analyzed and compared with the data from potentiostat to evaluate the quality of the cosine current perturbation and the accuracy of voltage/current readings collected.

3.3 Experiment 2. B_{phone} Estimation

The experiment set-up is the same as experiment 1. Since the phone is powered at a constant voltage 3.9V. The current readings measured by the potentiostat depend on input opaqueness signal and B_{phone}. The current behavior at different frequencies can be analyzed to estimate the phone transfer function that links screen opacity to current, without any battery voltage modulation at any frequency.

3.4 Experiment 3. Accurate measurement of $Z_{battery}$

We use a Solartron Analytical 1287 Electrochemical interface combined with Model 1250B Frequency Response Analyzer to do EIS measurement on the EV-30 battery at 50% SOC reported by the phone. Four terminals of the Model 1287A, counter electrode, working electrode and two reference electrodes, are used to eliminate the errors caused by wire and contacting resistance. Current perturbations with zero mean current and non-zero mean current were used. Impedance results are furthermore analyzed by software ZView and used to build up ECM of the battery.

3.5 Experiment 4. Measurement of $Z_{battery}$ from the App

We use the App to do EIS measurements with the battery operating the phone, instead of the potentiostat. We charge or discharge the battery until 50% SOC is reported by the phone. The sampling rate is set to be 8 points per perturbation cycle to get a relatively wide frequency range and good data quality. The perturbation frequency ranges was from 2.2Hz to 0.1Hz. Because the battery is discharging during the experiments, low frequencies can lead to an appreciable decrease of SOC during a measurement.

Experimental data collected by the App is further analyzed with Matlab and ZView to derive the impedance spectrum and ECM of battery. The App results are compared to the experimental results from experiment 3, the App performance is evaluated. Results are also used to validate the pseudo-current perturbation.

4. Results and Discussion

4.1 Current Perturbation Design

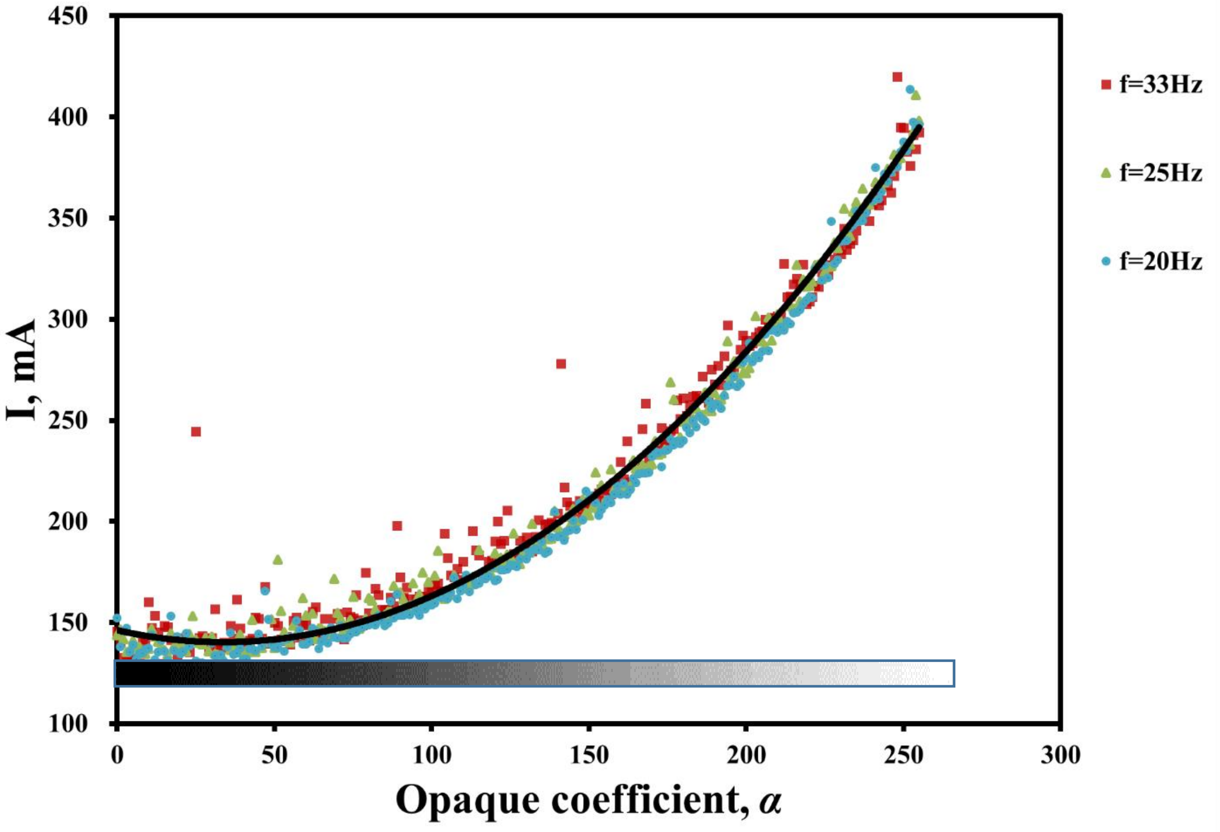

Figure 7. The relationship between α values and phone current readings, sampling at 20Hz, 25Hz and 33Hz.

It can be observed that the phone current is proportional to α values. Low current readings around 150mA are recorded in the region of 0 - 70 α units. This is a situation where the screen is dark. The highest current readings around 400mA are recorded at 255 α, when the screen is fully bright.

All three sets of data at different frequencies are fitted into second order polynomials as:

$$I = a * \alpha^2 + b * \alpha + c \tag{27}$$

Where, a, b and c are coefficients; α is the opaque coefficient.

Frequency	a	b	c	R^2
33Hz	0.0047	-0.2446	146.1724	0.9778
25Hz	0.0052	-0.3501	146.1852	0.9917
20Hz	0.0054	-0.4087	144.7671	0.9949
Average	0.0051	-0.3345	145.7082	

Table.1. Spreadsheet of polynomials coefficients.

According to Table 1, second order polynomials give excellent fit with variance close to 1. As sampling frequency decreases, the variance is getting closer to 1, which indicates a better fit. Since sampling at higher frequency means driving the CPU more aggressively, the stability of the phone system is affected, which leads to more dispersive current readings on Figure 7. At the same time, all three coefficients are varying with sampling frequencies because different sampling frequencies contribute to different usage of CPU.

Ideally, fitted polynomials for the full sampling frequency range from 01.Hz to 33Hz can be calculated. The α values needed to excite a cosine for each frequency can be solved from equation:

$$a * \alpha^2 + b * \alpha + c = I_o + \Delta I * cos(\omega t) \tag{28}$$

However, it is time consuming and raises the complexity by assigning different set of α values to the App from a big database for each frequencies. As an initial trial, average coefficients are used in this thesis.

It is difficult to get an analytical solution for equation (28). However, for a specific point on a specific cosine, the right hand side of equation (28) become constant, and α can be solved easily from a second order equation. The general current range for screen fluctuate from black to white is 150-400mA. The current perturbation is designed to be a cosine at a mean current of 260mA with a magnitude of 100mA.

$$I = 260 + 100 * cos(\omega t) \tag{29}$$

32 points per cycle are used to describe the cosine, which provides good resolution. Then,

$$I = 260 + 100 * \sum_{i=0}^{i=31} cos\left(\frac{2\pi i}{32}\right) \tag{30}$$

The equation can be expressed as:

$$0.0052 * {\alpha_i}^2 - 0.3345 * \alpha_i + 145.7082 - 260 - 100 * cos\left(\frac{2\pi i}{32}\right) = 0, \quad i = 0, 1, 2 \cdots 31 \qquad (31)$$

All 32 points can solved step by step.

4.2 Results of Validation Tests of the App

4.2.1 Accuracy of the Sampling Frequency

Basic signal processing standards must be understood if we hope to use a self-driven cell phone to do EIS. For example, reliable digital waveform sampling is required. The time interval between two sampling points are inspected to get at this issue. Since the App is designed to record the current time when voltage/current readings are saved, the time interval between any two adjacent sampling points can be calculated. Statistics of time interval is applied for all data collected by the phone. Histograms of time interval deviation from the set value for different perturbation and sampling frequencies are investigated. Examples are shown in Figure 8 for several dfferent sampling frequencies.

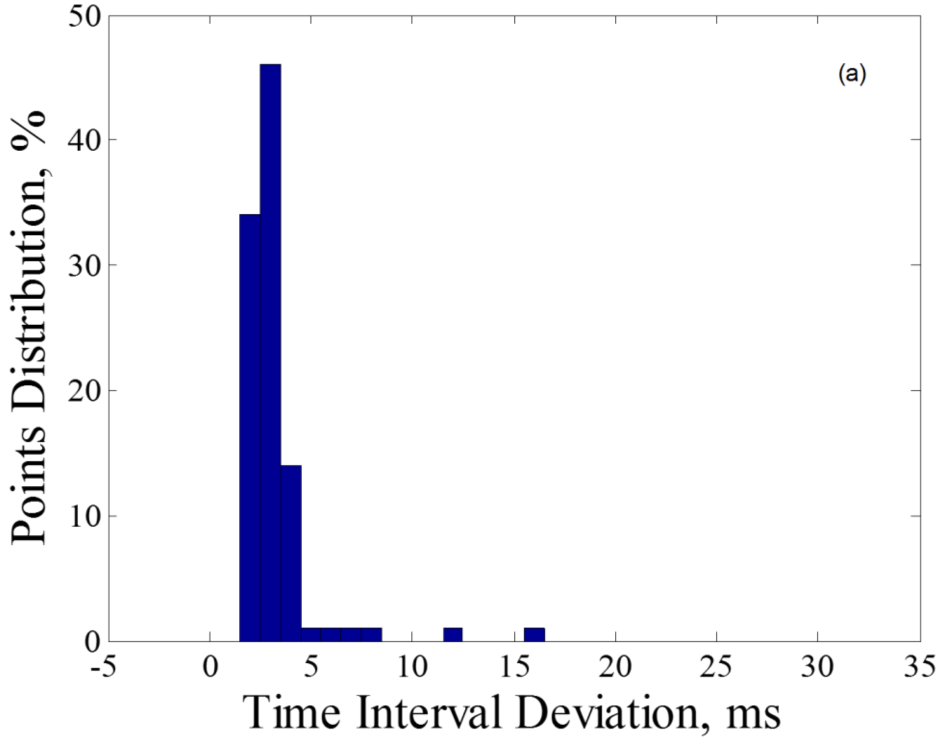
(a)
Points Distribution, %
0
10
20
30
40
50
-5
0
5
10
15
20
25
30
35
Time Interval Deviation, ms

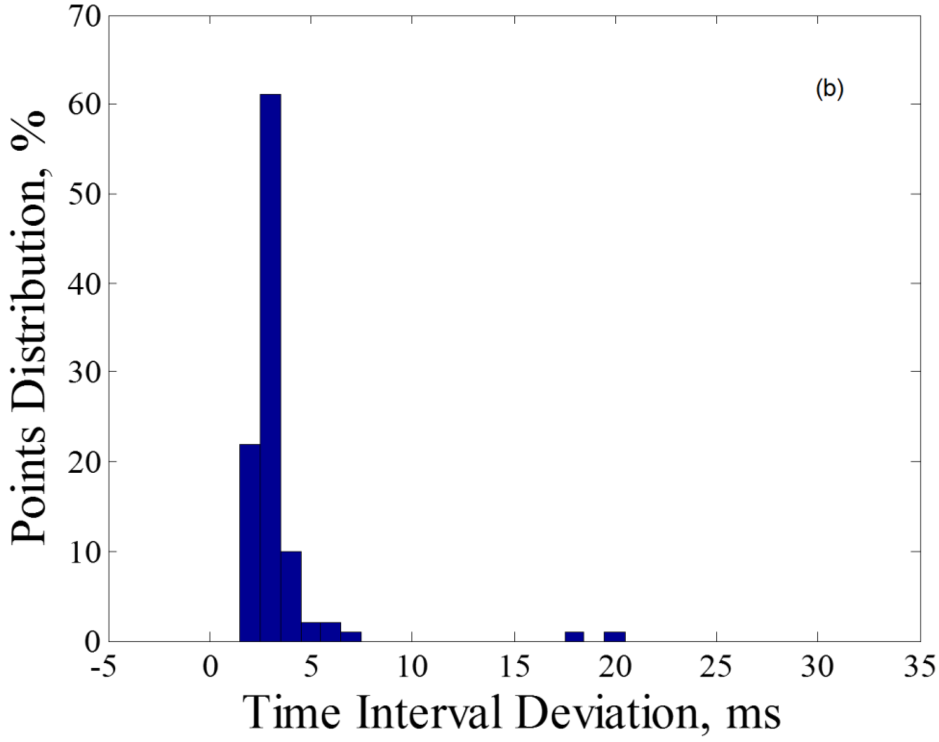
(b)
Points Distribution, %
0
10
20
30
40
50
60
70
-5
0
5
10
15
20
25
30
35
Time Interval Deviation, ms

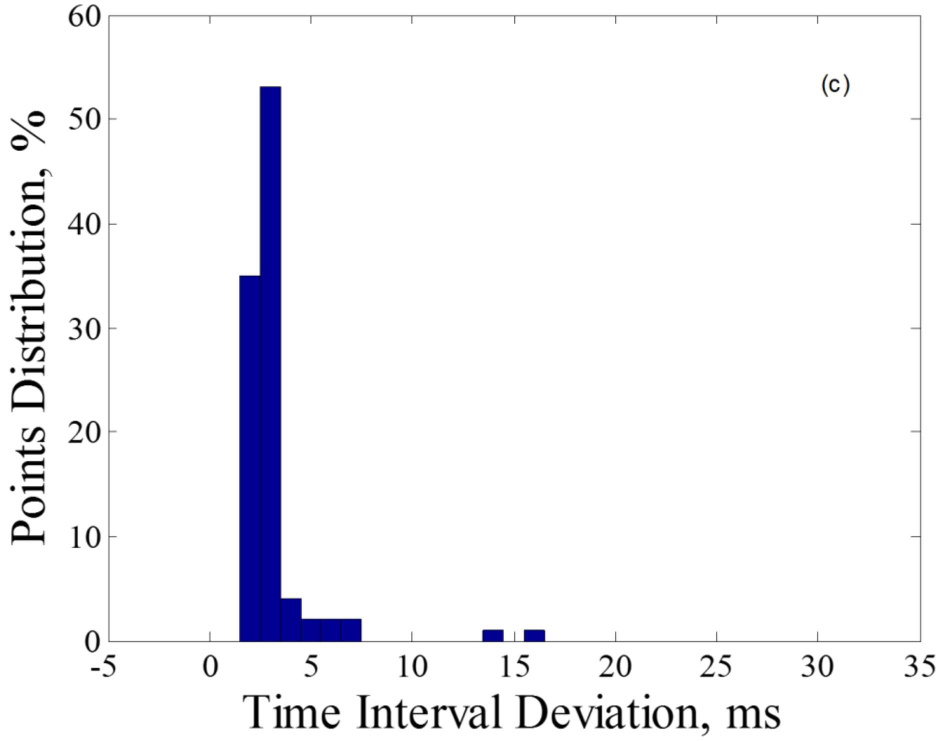
(c)
Points Distribution, %
Time Interval Deviation, ms
0
10
20
30
40
50
60
-5
0
5
10
15
20
25
30
35

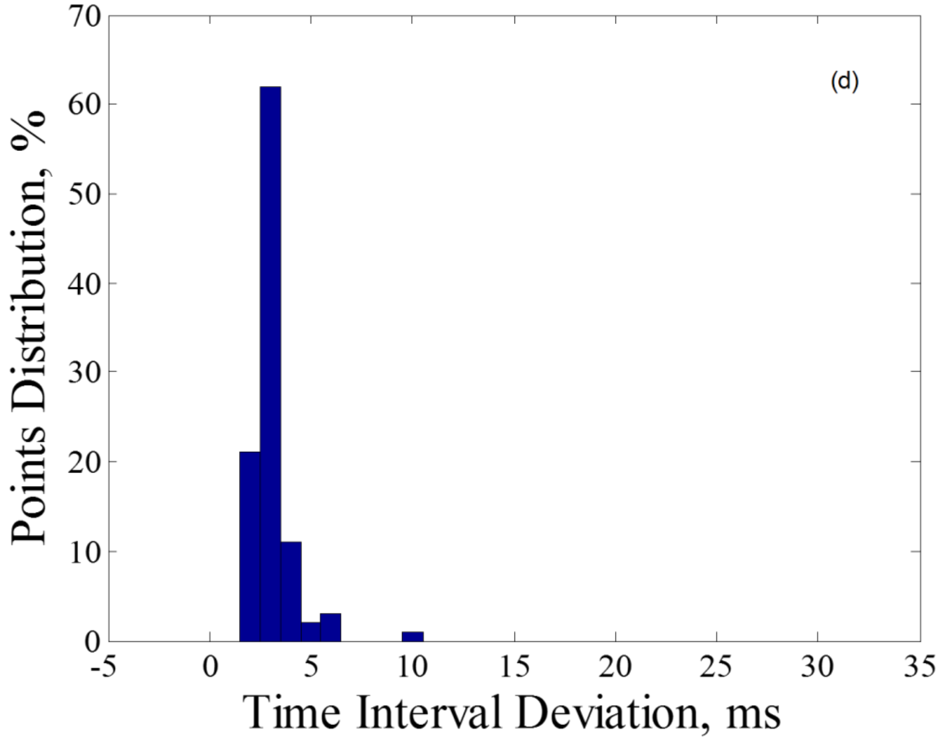
(d)
Points Distribution, %
Time Interval Deviation, ms
0
10
20
30
40
50
60
70
-5
0
5
10
15
20
25
30
35

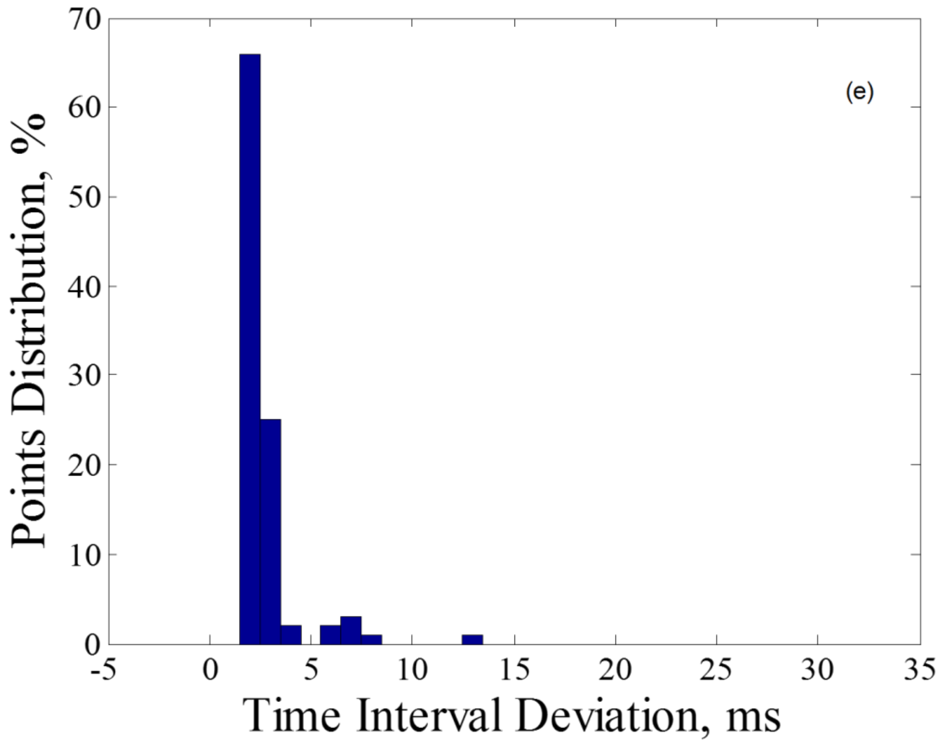

Figure. 8. Histograms of time interval deviation from set values. Sampling at (a) 8Hz, (b) 4Hz,(d) 2Hz, under 0.5Hz current perturbation; (c) 8Hz, under 1Hz current perturbation; (e) 8Hz, under 2Hz current perturbation.

A 2 ms systematic deviations between the set sampling interval and the actual on-board sampling interval is always seen. The deviation is due to the time delay between the App sending out request and the phone starting to response. In other words, the phone system needs at least 2ms to process the commands and take actions no matter how fast the App is asked to sample.

More than 98% of the timing deviations are in the range of 2-7ms, and more than 80% of deviations are either 2ms and 3ms. Deviations larger than 10ms are likely caused by other processes running in the background during measurement so it is important to have the phone foreground and background Apps in a known state before self-testing. After remove the large errors from random foreground and background processes, the distribution of timing deviations is calculated for each frequency. For (a), (c) and (d) in Figure 8 with the same 8Hz sampling frequency, the mean value of deviations decreases from 2.94ms to 2.87ms, then 2.58ms seen as perturbation frequency rises from 0.5Hz to 1Hz, then to 2Hz. Possible reason is that when the App is running the current perturbation at higher frequency, it will request more usage of CPU and RAM from the phone system, which forces the phone system to stop some other background processes to meet the request from the App. Then, the phone can react faster to the App.

For (d),(b) and (a) in Figure 8 with the same 0.5Hz current perturbation frequency, the mean value of deviations changes from 2.98ms to 3.01ms, then 2.94ms as sampling frequency rises from 2Hz to 4Hz, then to 8Hz. The differences between mean values are less than 0.1ms, which indicates that the influence from the sampling frequency on the accuracy of time interval can be neglected. Sampling at 8Hz correspond to reading and saving data every 125ms. In contrast, perturbing the current at 8Hz correspond to changing the α value every 4ms, which is 30 times faster than the sampling action.

System time delays result in inaccurate sampling, which propogates errors into the Fourier Transform results. In order to minimize the negative influence, we make a 3ms as compensation. For example, for 0.5 Hz current perturbation, if 8 sampling points per cycle is needed, the sampling frequency should be 4Hz. Hence, the time interval set in the App should be 247ms. However, the actual time interval is still varying at 250ms, since the system time delay is not a constant. This error is unavoidable but could be minimized if the CPU of the phone is powerful enough to respond to request at constant speed. In short, there is a complex interplay between the perturbation frequency and data sampling frequency. However, in all cases, that digitized data has a predictable and fairly tight sampling error that makes it suitable for FFT analysis and EIS diagnostics using the built in chipset and processor on this phone.

4.2.2 Quality of current perturbation excited by the App.

The current readings from the potentiostat are further inspected. The quality of the cosine current perturbation can be judged visually by the wave form, as a first approximation. After applying Fourier Transform, the consistency of set frequency and signal frequency revealed on the amplitude spectrum is inspected. The amplitude spectrum of the signal is calculated by:

$$\Delta \mathrm{I} = 2 * |\mathrm{FFT}(\mathrm{I})| \tag{32}$$

where, *FFT* stands for Fast Fourier Transform. Examples are shown in Figure 9-11.

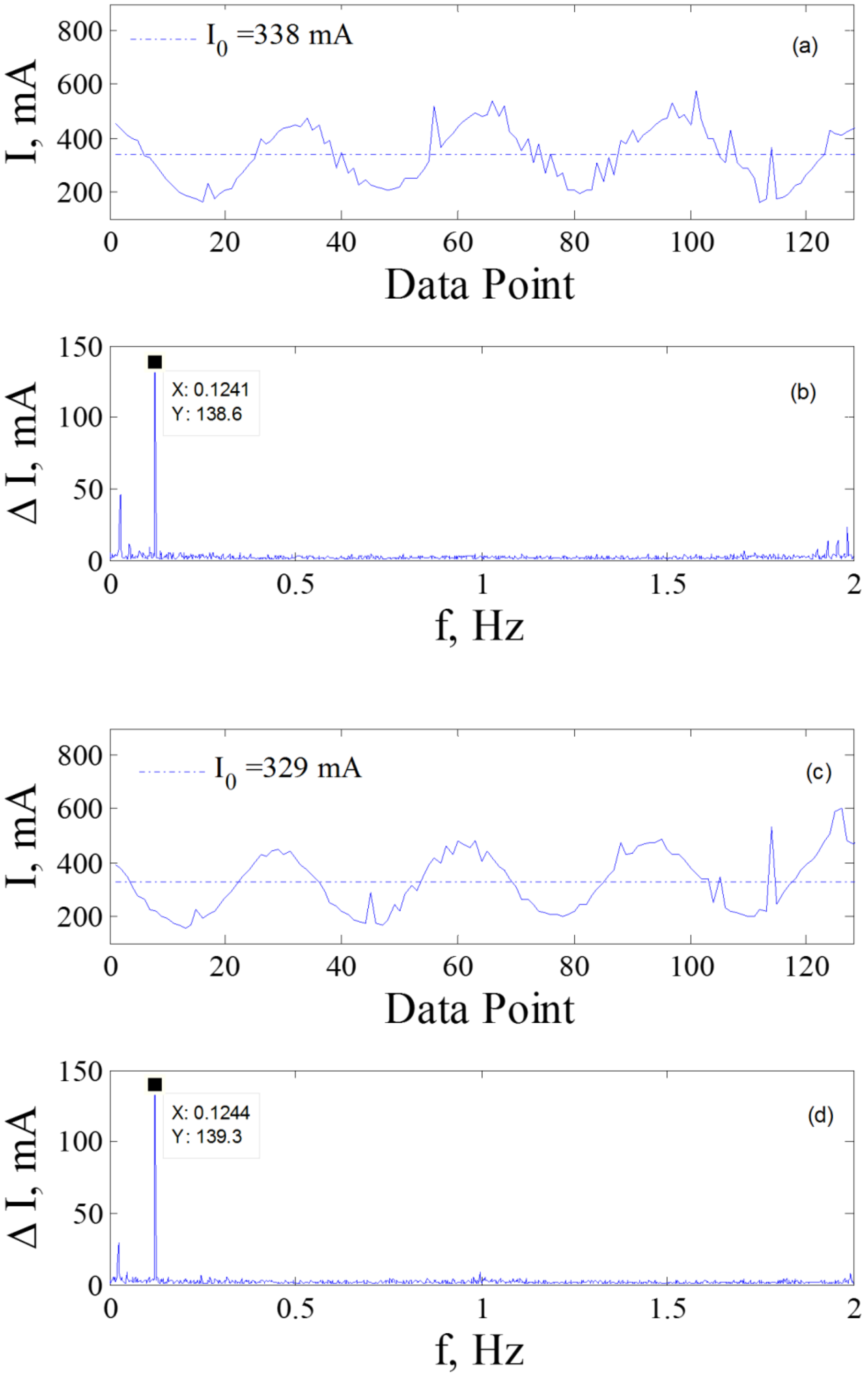
(a)
I_0 =338 mA
I, mA
800
600
400
200
0
20
40
60
80
100
120
Data Point
(b)
X: 0.1241
Y: 138.6
Δ I, mA
150
100
50
0
0.5
1
1.5
2
f, Hz
(c)
I_0 =329 mA
I, mA
Data Point
(d)
X: 0.1244
Y: 139.3
Δ I, mA
f, Hz

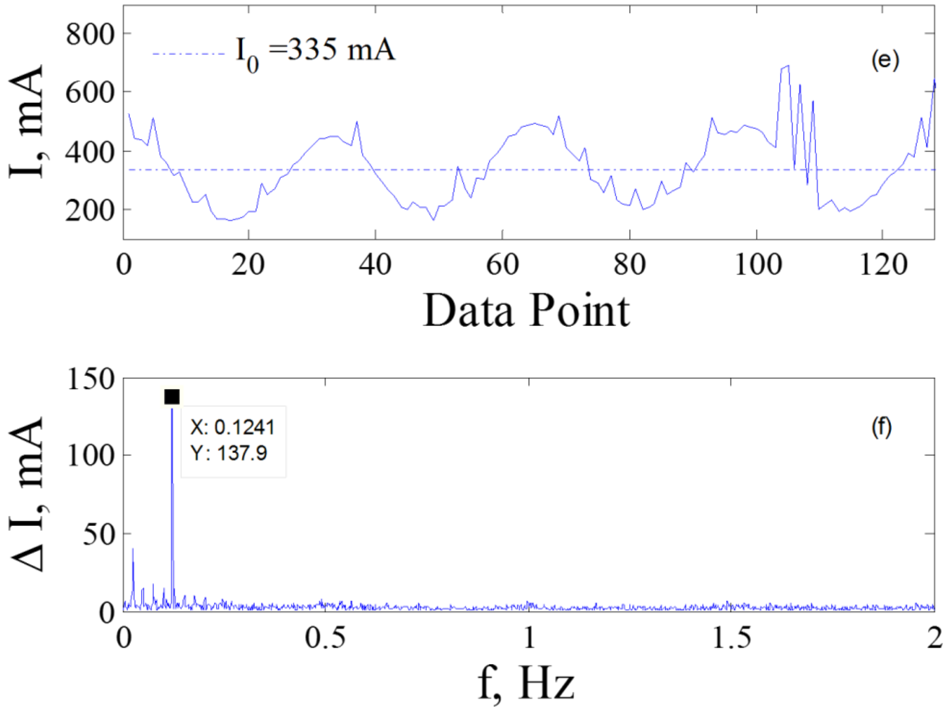

Figure 9. Current signal and amplitude spectrum for 0.125 Hz current perturbation and (a) (b) 2Hz, (c)(d) 1Hz, (e)(f) 0.5Hz phone sampling frequency.

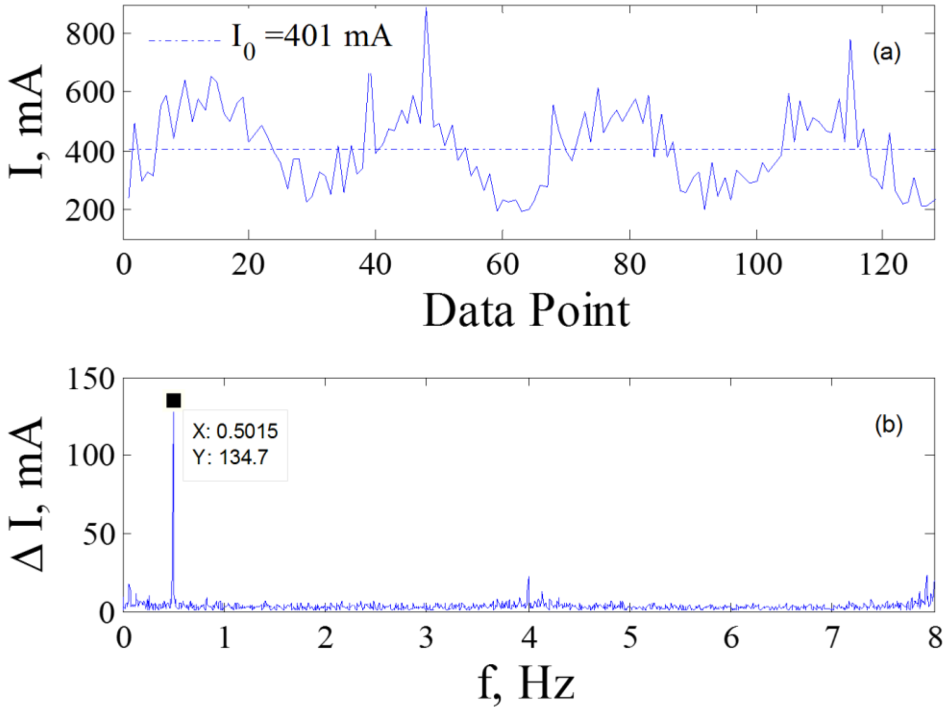

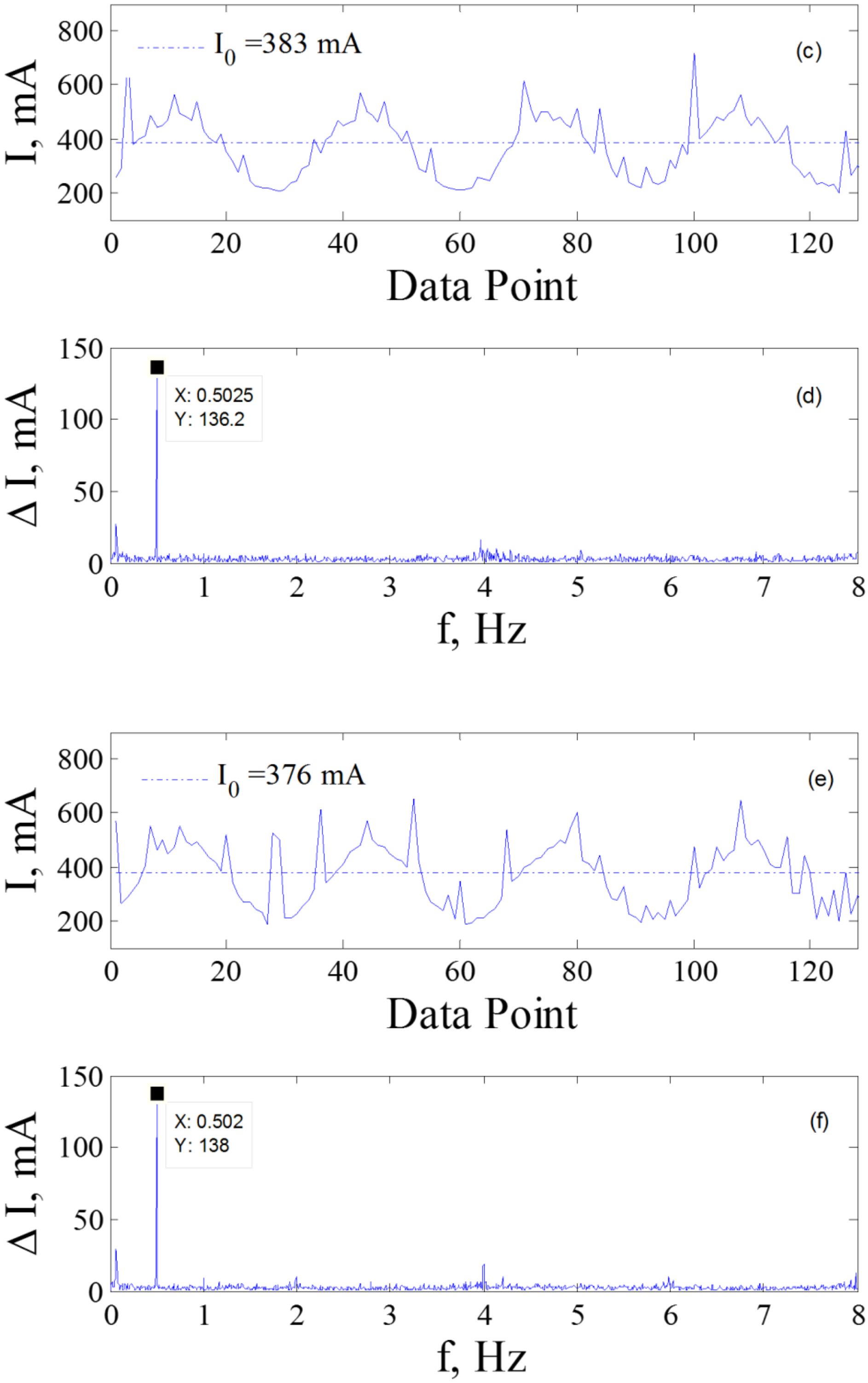

Figure 10. Current signal and amplitude spectrum for 0.5 Hz current perturbation and (a) (b) 8Hz, (c)(d) 4Hz, (e)(f) 2Hz phone sampling frequency.

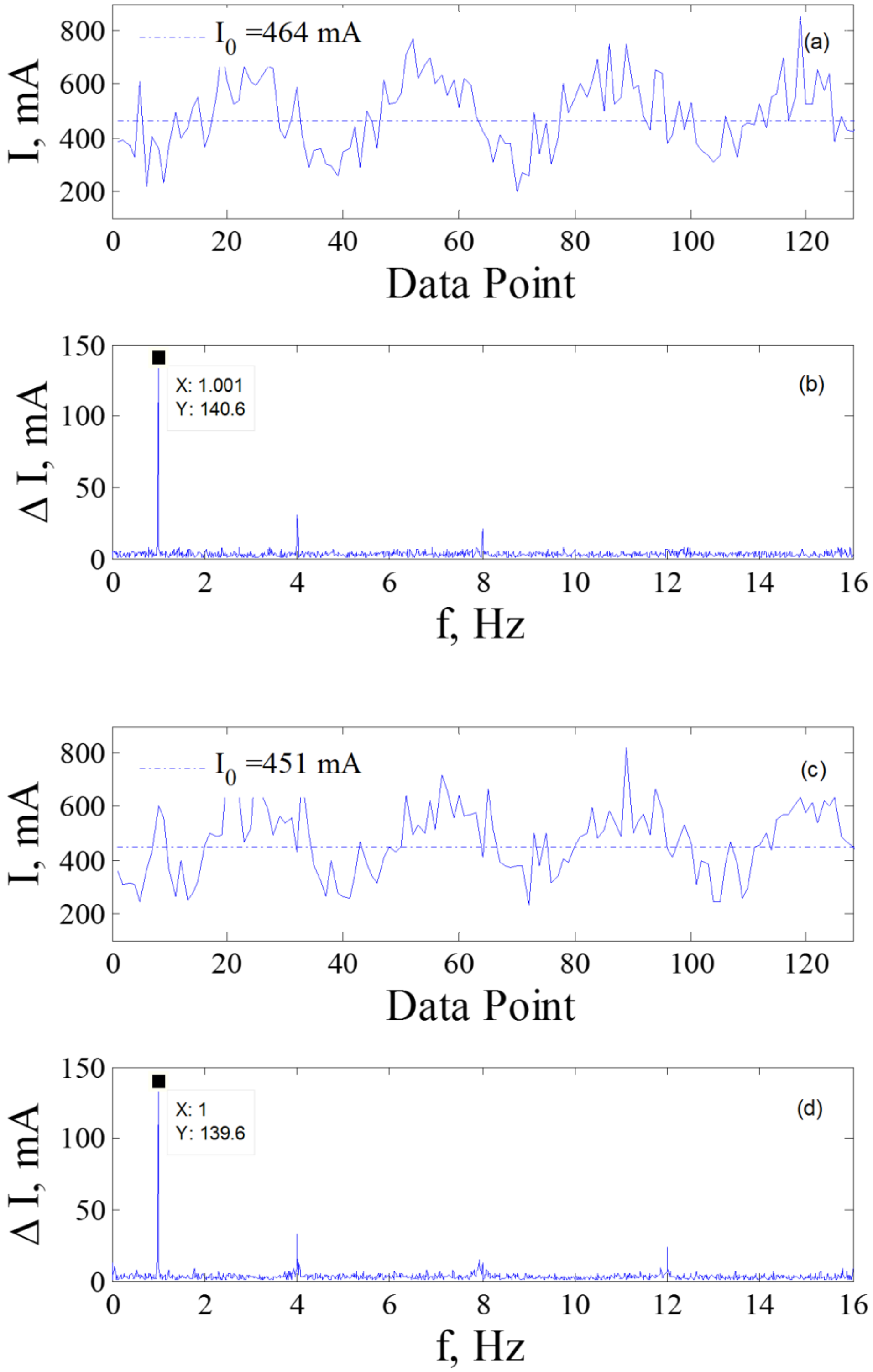
I, mA
800
600
400
200
I$_0$ =464 mA
(a)
0
20
40
60
80
100
120
Data Point
Δ I, mA
150
100
50
0
X: 1.001
Y: 140.6
(b)
0
2
4
6
8
10
12
14
16
f, Hz
I, mA
800
600
400
200
I$_0$ =451 mA
(c)
0
20
40
60
80
100
120
Data Point
Δ I, mA
150
100
50
0
X: 1
Y: 139.6
(d)
0
2
4
6
8
10
12
14
16
f, Hz

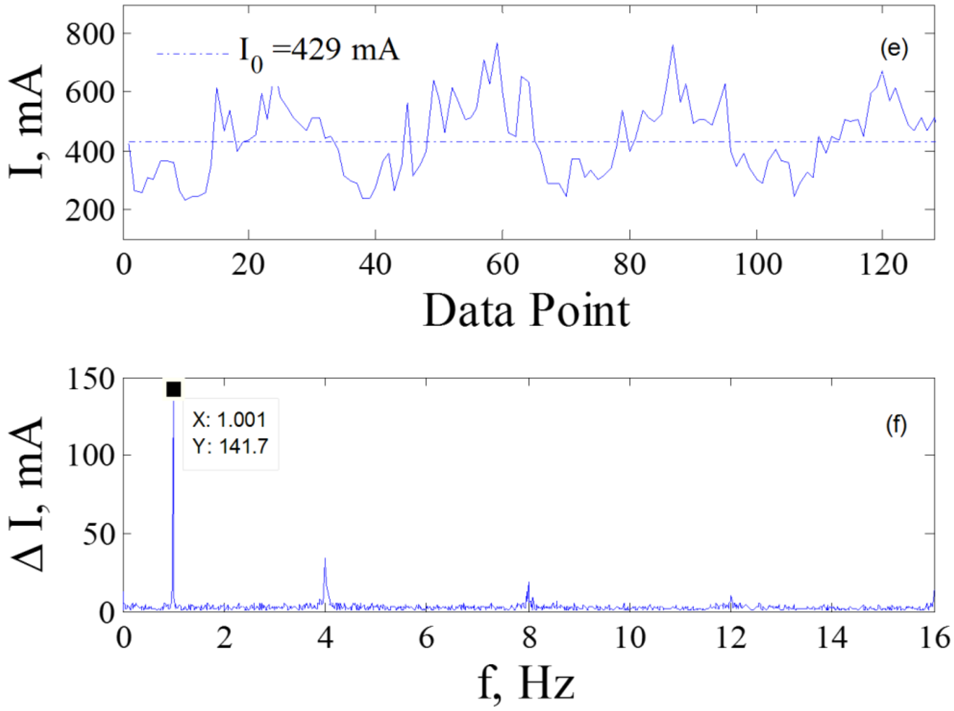

Figure 11. Current signal and amplitude spectrum for 1 Hz current perturbation and (a) (b) 16Hz, (c) (d) 8Hz, (e) (f) 4Hz phone sampling frequency.

Based on visual judgment of (a), (c) and (e) in Figure 9 and Figure 10, the wave form of current signal at 0.125Hz and 0.5Hz are good cosine waves with noise. In Figure 11, the waveform of signals shown in (a), (c) and (e) are polluted by noise that cannot be identified as a cosine wave. However, by inspecting into (b), (d) and (f) in Figure 9-11, the highest peak in each amplitude spectrum clearly indicates the existence of the first order harmonic at 0.125Hz, 0.5Hz and 1Hz respectively, which proves that the current signal is a periodic signal at set frequency. The deviation of the observed signal frequency on the amplitude spectrum from the set value is due to the inconsistent sampling time interval discussed above. Based on the judgement of wave form and observation in the amplitude spectrums, current perturbations excited by the App can be considered as good cosine signal. The amplitude of the current signal for different frequencies are presented in Figure 12 (b), (d) and (f). From 0.125 Hz to 1.25Hz, 2.5Hz and 4Hz, the amplitude maintains at 140mA, which indicates that current perturbations are stable at different frequencies.

In Figure 10, it can be observed that the mean current increases from 376mA to 401mA as the phone sampling frequency increases from 2Hz to 8Hz. In Figure 11, the mean current increases from 429mA to 464mA as the sampling frequency increases from 4Hz to 16Hz. Faster sampling speeds drive more usage of CPU and that results in more current consumption. But, mean currents stay at approximately the same level of 330mA for difference frequencies in Figure 9, because sampling frequencies from 0.5 to 2Hz are relatively low frequencies, and they do not drive the CPU aggressively enough to make significant changes to the mean currents.

By comparing Figure 9(a) with Figure 10(e), it can be observed that when sampling at 2Hz, the mean current increases from 338mA to 376mA as the current perturbation frequency increases from 0.125Hz to 0.5Hz. In Figure 10(c) and Figure 11(e), when sampling at 4Hz, the mean current increases from 383mA to 429mA as the current perturbation frequency increases from 0.5Hz to 1Hz. In analogy to the discussion above, more aggressive perturbation would contribute to higher usage of CPU leading to higher mean current. Hence, both the sampling frequency and perturbation frequency will affect the mean current during experiments. Mean current at different perturbation frequency with 16, 8, and 4 sampling points per current perturbation cycle are shown in Figure 13 (b), (d) and (f), which further illustrate the dependency of mean current on sampling and perturbation frequency.

Although, the real mean current and amplitude are different from the set values in our original solution to the alpha equation, $I_0 = 260\text{mA}, \Delta I = 100\text{mA}$ in section 4.1, it is convincing to consider the current perturbation excited by the App as a good cosine signal source in the frequency range used in our experiments according to the analysis.

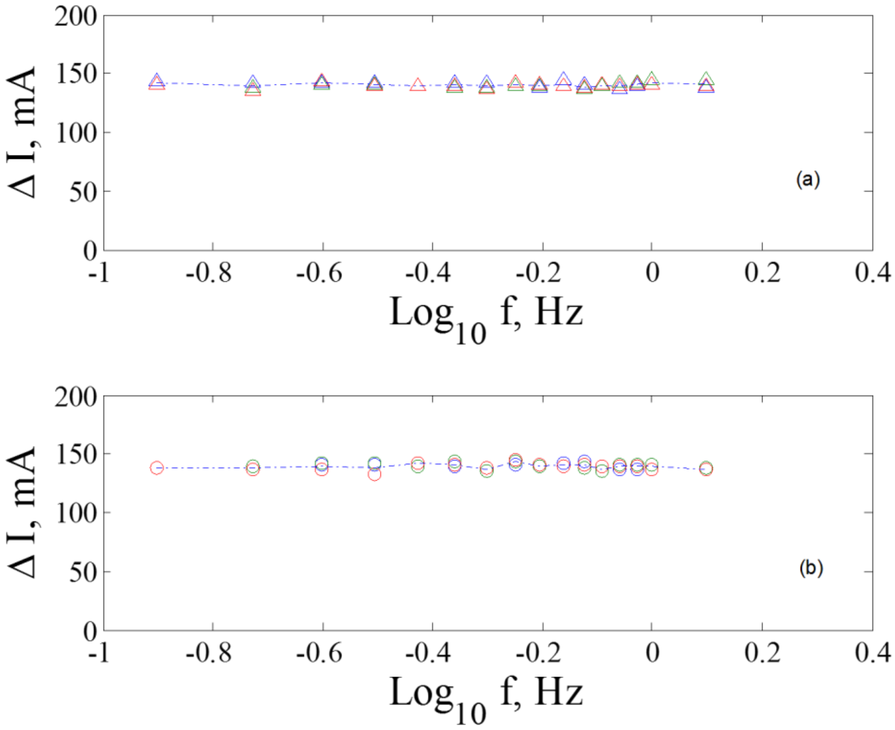

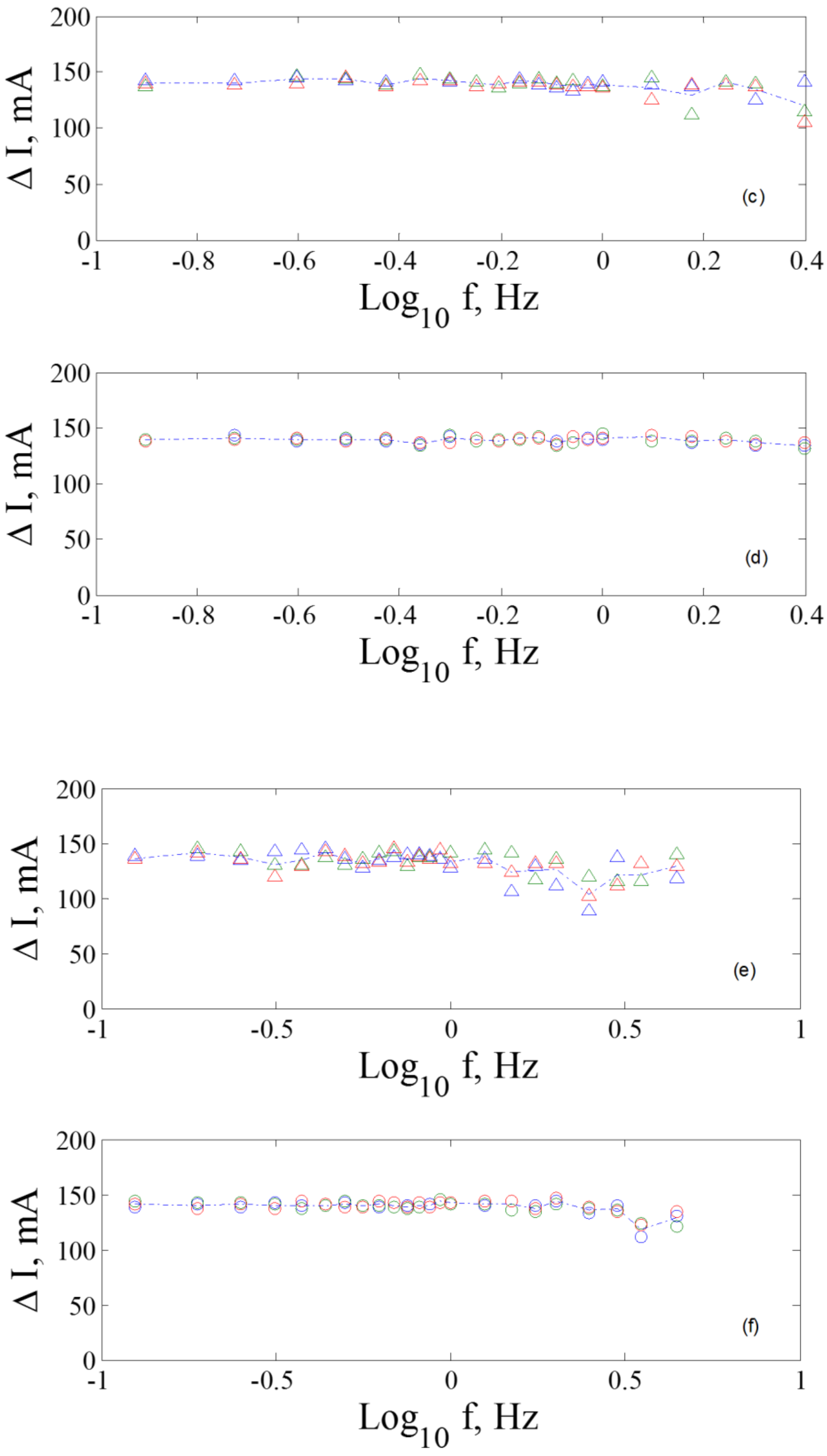

Figure 12. Current amplitude spectrum from the potentiostat sampling at (b)(d)(f) 32 points per cycle, and from the phone sampling at (a)16 points, (b)8 points,(c) 4points per cycle.

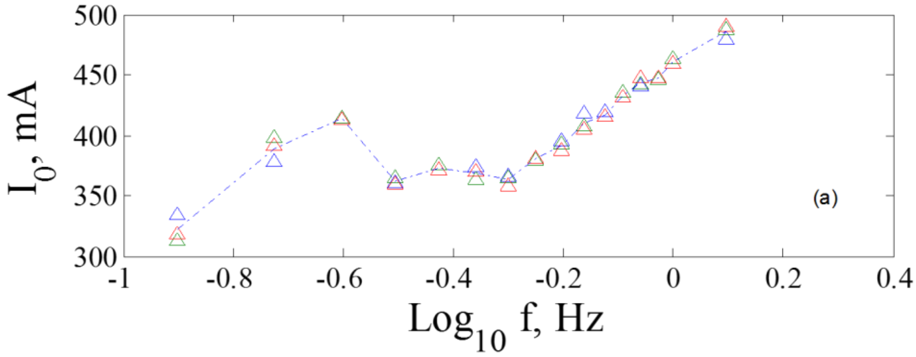
I$_0$, mA
500
450
400
350
300
-1
-0.8
-0.6
-0.4
-0.2
0
0.2
0.4
Log$_{10}$ f, Hz
(a)

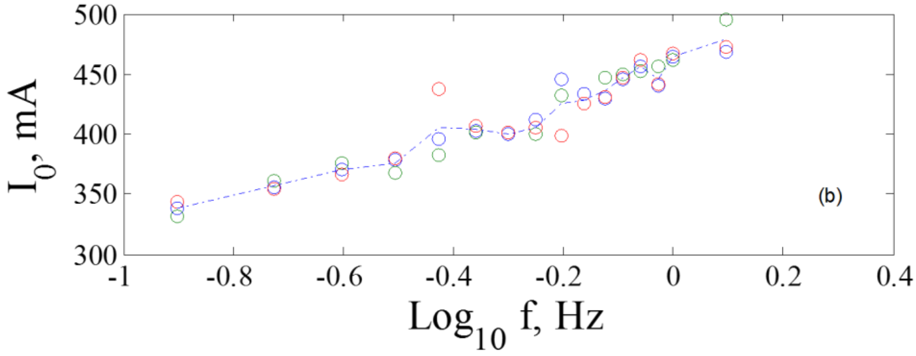
I$_0$, mA
500
450
400
350
300
-1
-0.8
-0.6
-0.4
-0.2
0
0.2
0.4
Log$_{10}$ f, Hz
(b)

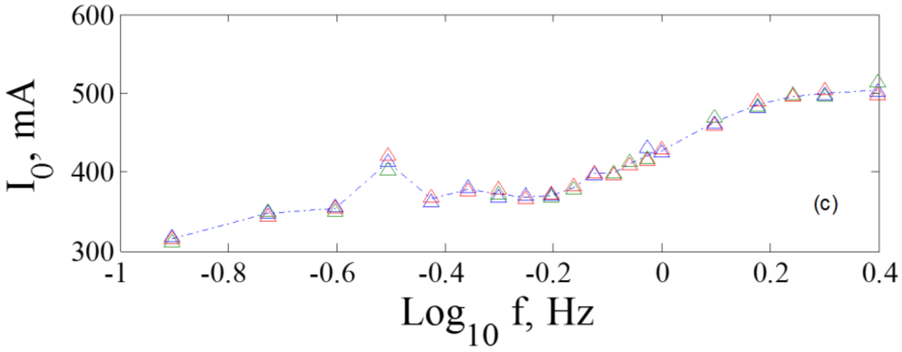
I$_0$, mA
600
500
400
300
-1
-0.8
-0.6
-0.4
-0.2
0
0.2
0.4
Log$_{10}$ f, Hz
(c)

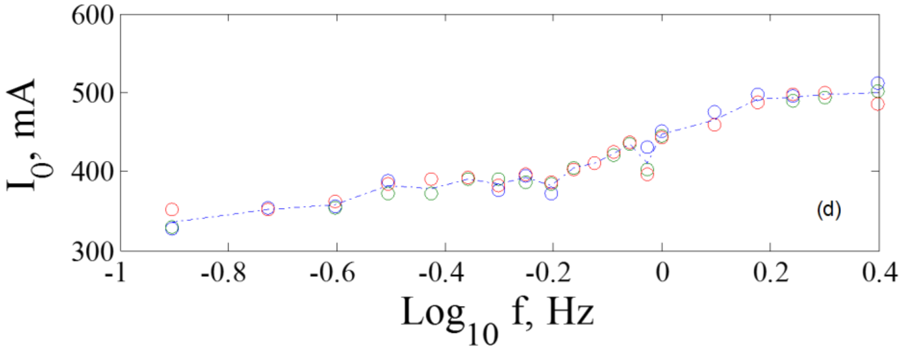
I$_0$, mA
600
500
400
300
-1
-0.8
-0.6
-0.4
-0.2
0
0.2
0.4
Log$_{10}$ f, Hz
(d)

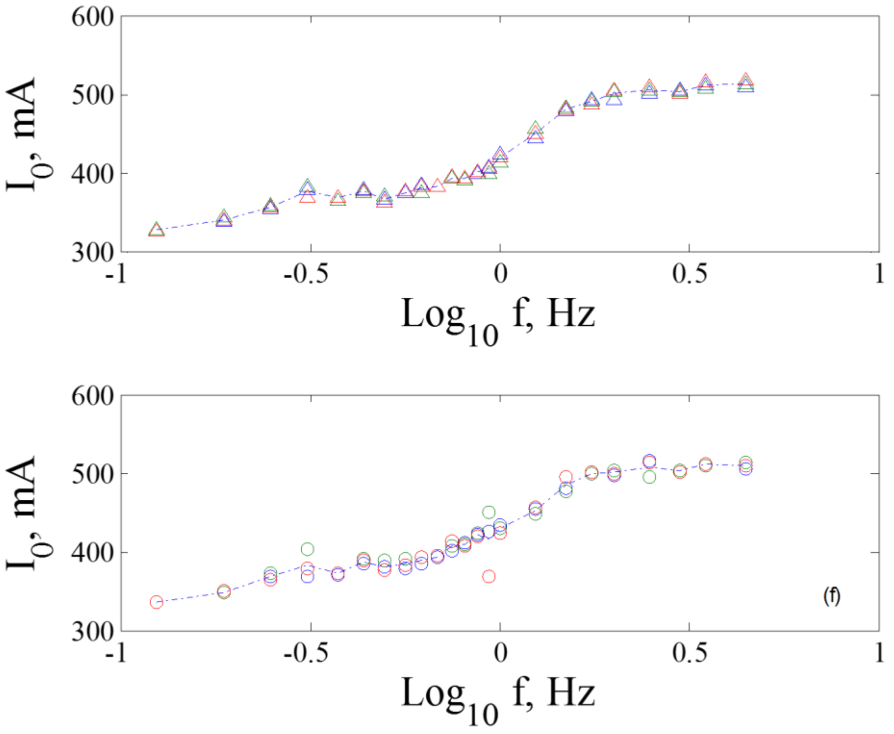

Figure 13. Mean current spectrums from the potentiostat sampling at (b) (d) (f) 32 points per cycle, and from the phone sampling at (a) 16 points, (b) 8 points, and (c) 4 points per cycle.

4.2.3 Quality of phone readings

The quality of phone readings is judged in a similar scenario to section 4.2.2 except that the current signal inspected is collected from the phone rather than the potentiostat. The waveform for the current signals and amplitude spectrums are shown in Figure 14 and Figure 15 as examples for discussion.

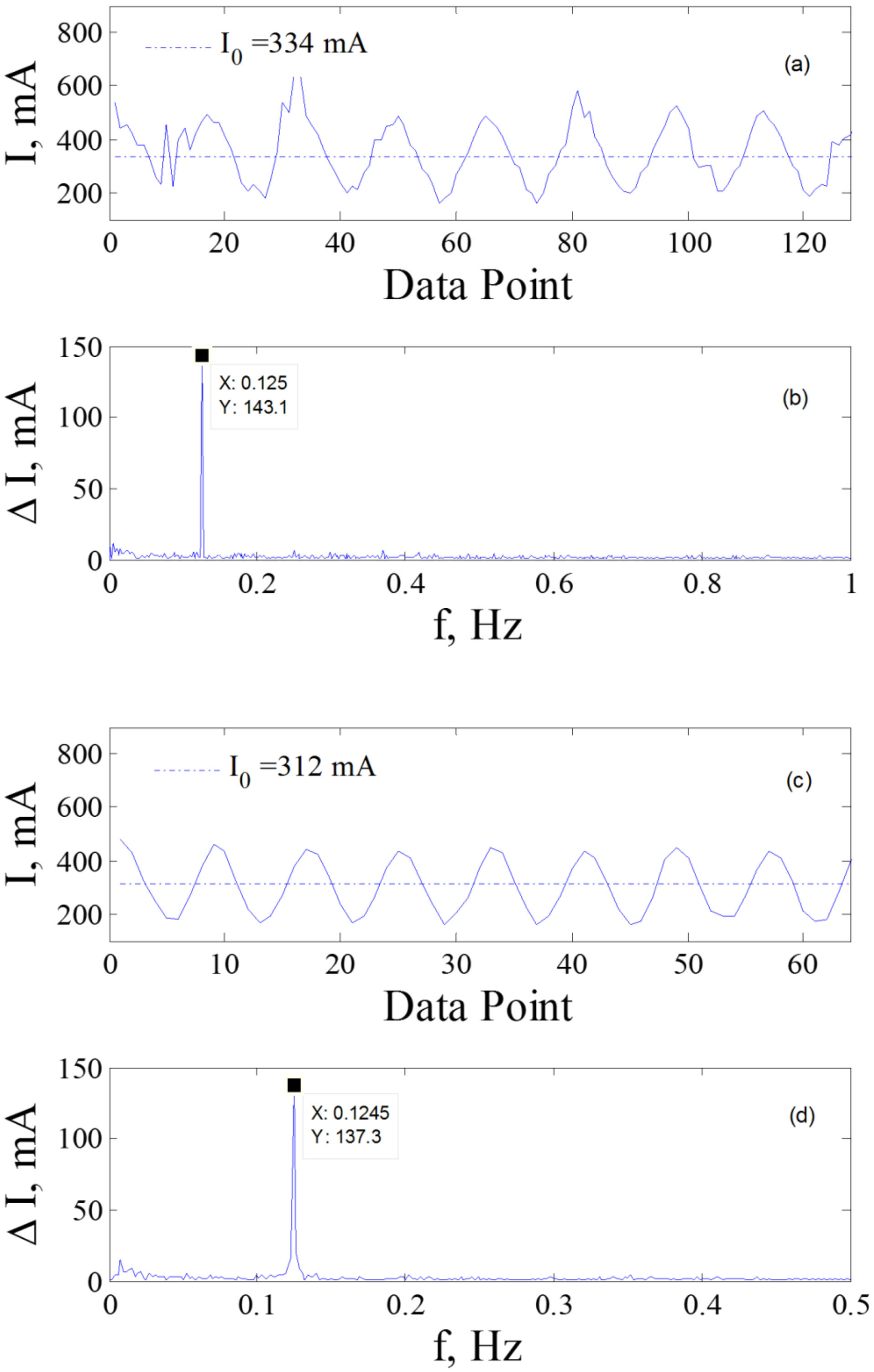
I, mA
800
600
400
200
I$_0$ =334 mA
(a)
0
20
40
60
80
100
120
Data Point
Δ I, mA
150
100
50
0
X: 0.125
Y: 143.1
(b)
0
0.2
0.4
0.6
0.8
1
f, Hz
I, mA
800
600
400
200
I$_0$ =312 mA
(c)
0
10
20
30
40
50
60
Data Point
Δ I, mA
150
100
50
0
X: 0.1245
Y: 137.3
(d)
0
0.1
0.2
0.3
0.4
0.5
f, Hz

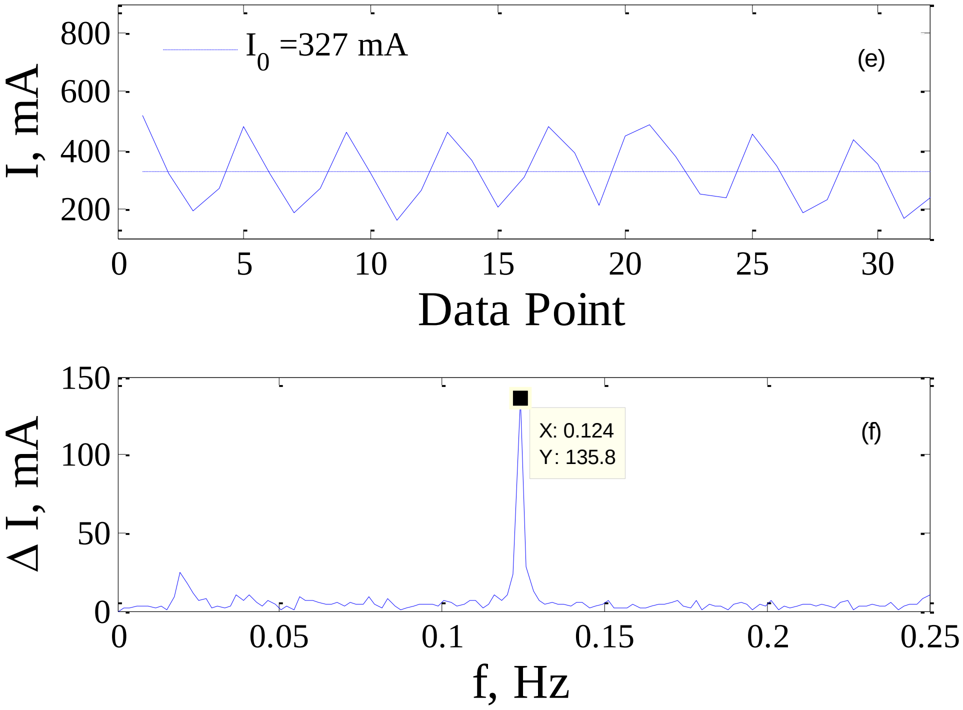

Figure 14. Current and amplitude data from phone with 0.125 Hz current perturbation at (a) (b) 2Hz, (c)(d) 1Hz, (e)(f) 0.5Hz phone sampling frequency.

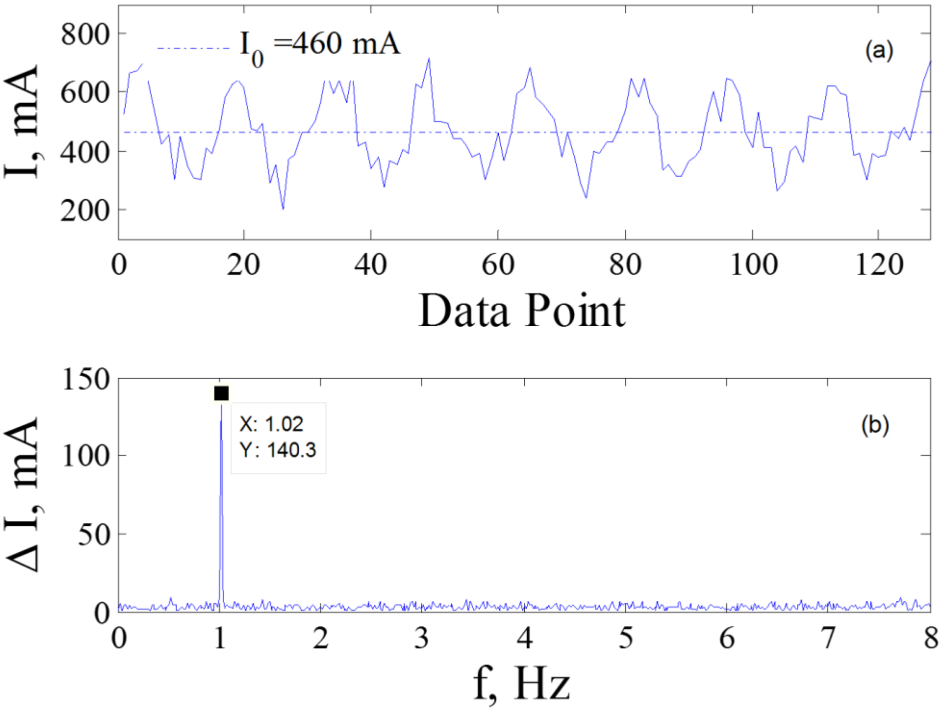

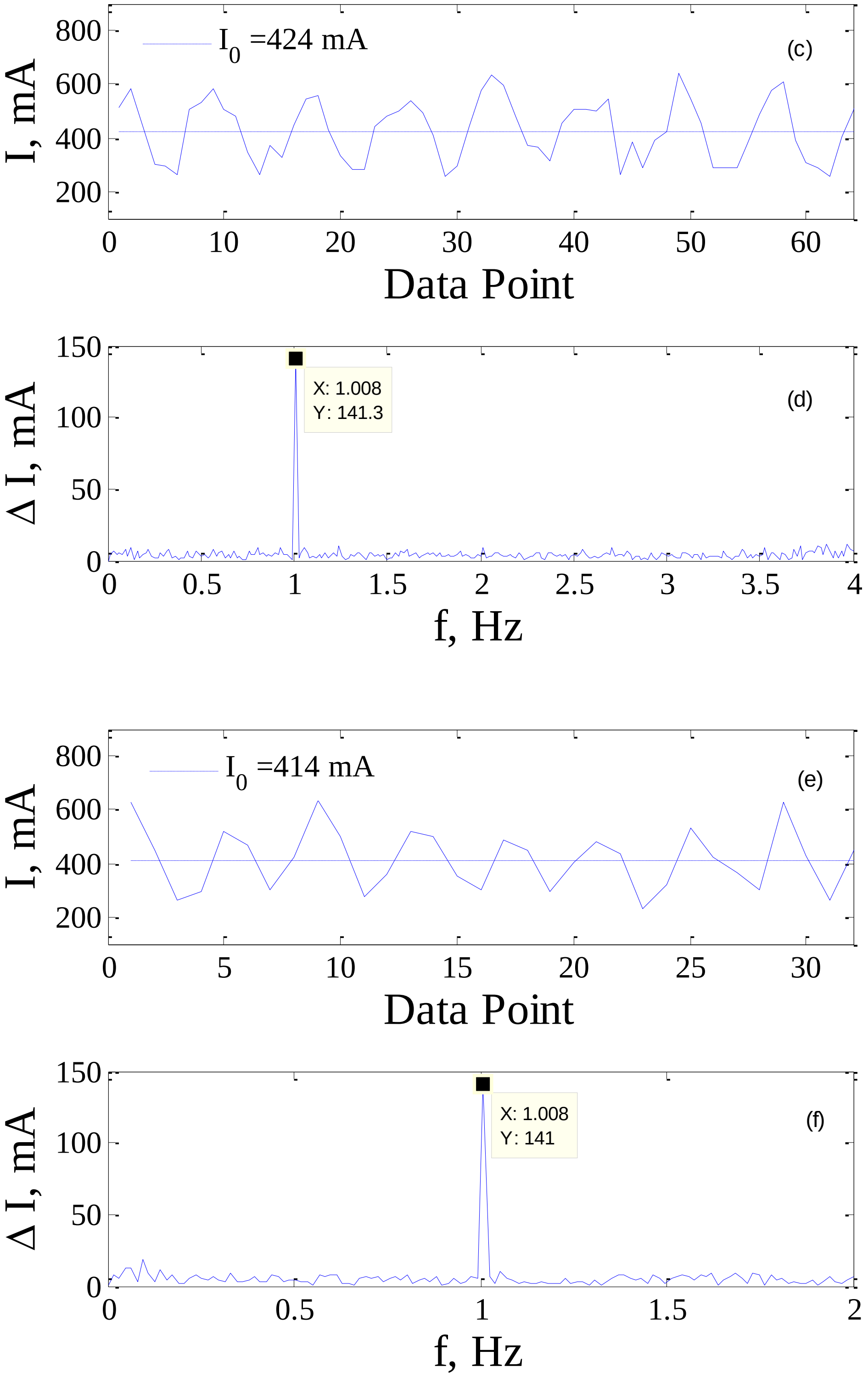

Figure 15. Current and amplitude data from phone with 1Hz current perturbation at (a) (b) 8Hz, (c)(d) 8Hz, (e)(f) 4Hz phone sampling frequency.

Based on visual judgment of (a), (c) and (e) on Figure 14, the current signals at

0.125Hz behave as good cosine signals with acceptable noise. In Figure 15, the wave form of signals shown in (a), (c) and (e) has significant noise involved. However, by inspecting into (b),(d) and (f) in Figure 14 and Figure 15, the highest peak in each amplitude spectrum clearly indicates the existence of the first order harmonic at 0.125Hz and 1Hz respectively, which are consistent with the results from potentiostat in Figure 10 and Figure 11. In addition, by comparing the mean current and the amplitude spectrums in Figure 12 and Figure 13 respectively, it can be observed that the current amplitude measured by the phone maintains steady at 140mA; the mean current has similar behaviors and tendency to the result from the potentiostat despite of possible noise introduced by other processes. Hence, it is relatively convincing to state that the data recorded by the phone is accurate and comparable to what we measure with the potentiostat.

4.2.4 $\mathrm{B_{phone}}$ Analysis

In Figure 12, the amplitude of current perturbation maintains at 140mA for different frequencies. Since we are using the same α perturbation format, the modulus of $\tilde{\alpha}$ is the same for all frequencies. The modulus of $\tilde{\mathrm{I}}$ is corresponding to the current amplitude calculated in Figure 12. Hence, the relationship between the screen modulation and current modulation does not change with perturbation frequency. It indicates that the phone transfer function $\mathrm{B_{phone}}$ is independent of the perturbation frequency according to the analysis in section 2.3. In Figure 13, the mean current is increasing as frequency, which indicates the dependency of $\mathrm{B_{phone}}$ on the mean current. But, mean current is not involved in calculating the battery impedance in equation (20). We can consider B_{phone} as a constant when measuring the $Z_{battery}$ from the phone.

4.3 $Z_{battery}$ Measurement with analytical instruments.

Two EIS experiments are tested on the EV-30 battery at 50% SOC in the lab: a 200mA amplitude current perturbation with zero mean current and the same perturbation with a 350mA mean current. The spectrum is from 0.1Hz to 500 Hz. Nyquist plots constructed with ZView software are shown in Figure 16.

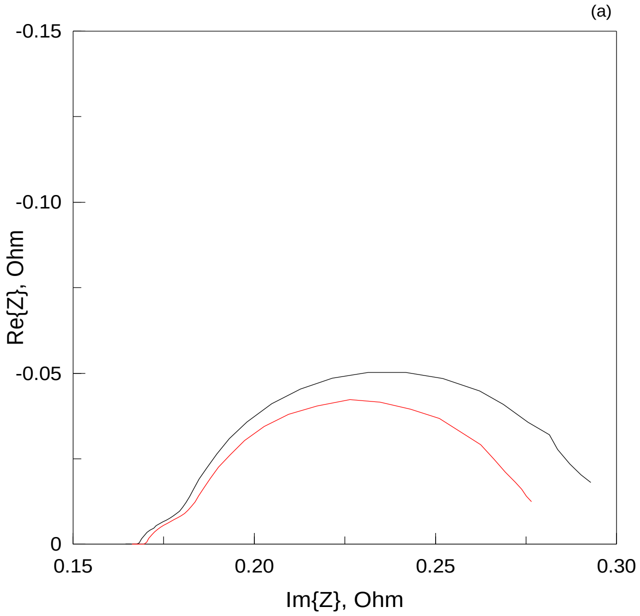

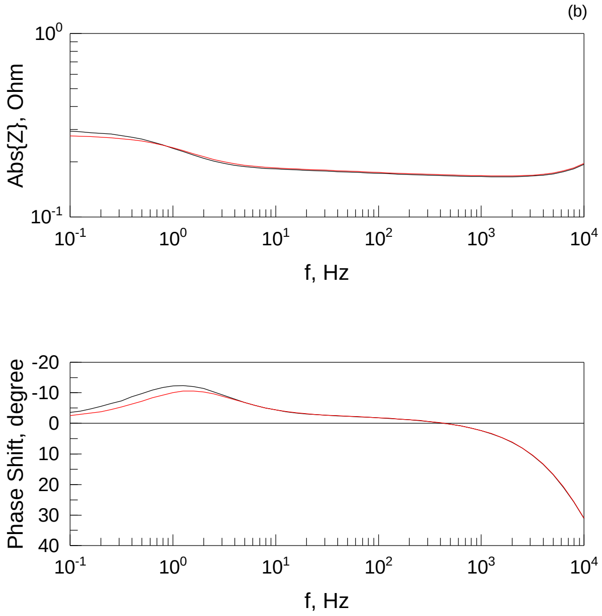

Figure 16. Impedance of EV-30 with 200mA perturbation at :(red line) zero mean, and (black line) 350mA mean current. (a) Nyquist plot (b) Bode plot.

The experimental frequency range is not low enough to reveal the Warburg impedance, nor high enough to reveal inductance, but it is adequate to determine the charge-transfer resistance and ohmic resistance. From visual inspection of Figure 16(a), the ohmic resistance R_0 and charge-transfer resistances at the negative electrode are about 0.16Ω and 0.02Ω for both mean current cases, but the charge-transfer resistances at the positive electrode depends on the mean current, and is 0.1Ω and 0.11Ω for zero mean current and 350mA mean current, respectively. Both impedance spectrums are fitted into ECM provided in section 2.1. Results are listed in Table 2.

Model:	$\boldsymbol{R_0}$(Ohm)	$\boldsymbol{R_{ct,p}}$(Ohm)	$\boldsymbol{C_{dl,p}}$(F)	$\boldsymbol{R_{ct,n}}$(Ohm)	$\boldsymbol{C_{dl,n}}$(F)
350mA Mean	0.16625	0.10756	1.589	0.015587	0.13339

Zero Mean	0.16808	0.089823	1.48	0.015473	0.1212

Table 2. Coefficients of elements in ECM.

Coefficients in Table 2 are consistent with the visual measurements on Nyquist Plots. Resistive and Capacitive elements stay at the same state with less than 8% difference except for c. A significant 19.7% increase in $R_{ct,p}$ is observed visually from Figure 16(a) and numerically from Table 2 from zero mean current to 350mA mean current. The same observation is mentioned in [19]. Since the battery keeps discharging at 350mA during EIS measurement, a decrease of SOC and drift of voltage occurs.

4.4 $\mathbf{Z_{battery}}$ Measurement with the App on the phone

Voltage and current readings are extracted from the phone and further analyze with Matlab FFT analysis. The example of time domain data is shown in Figure 17. Time domain data is transformed into frequency domain data by Fast Fourier Transform for analysis.

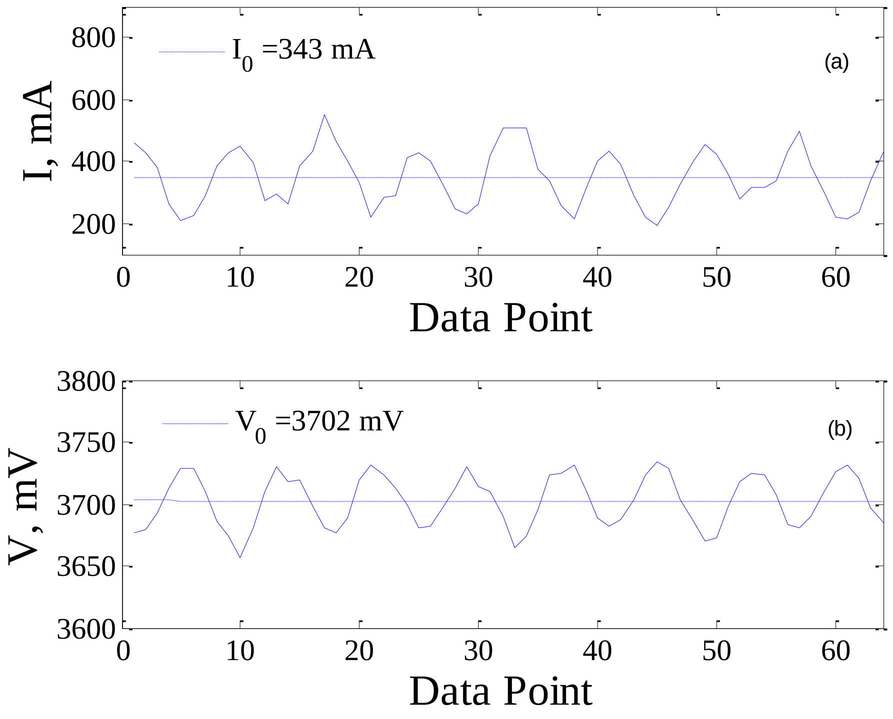

Figure 17, 0.5Hz (a) current readings and (b) voltage readings from the phone.

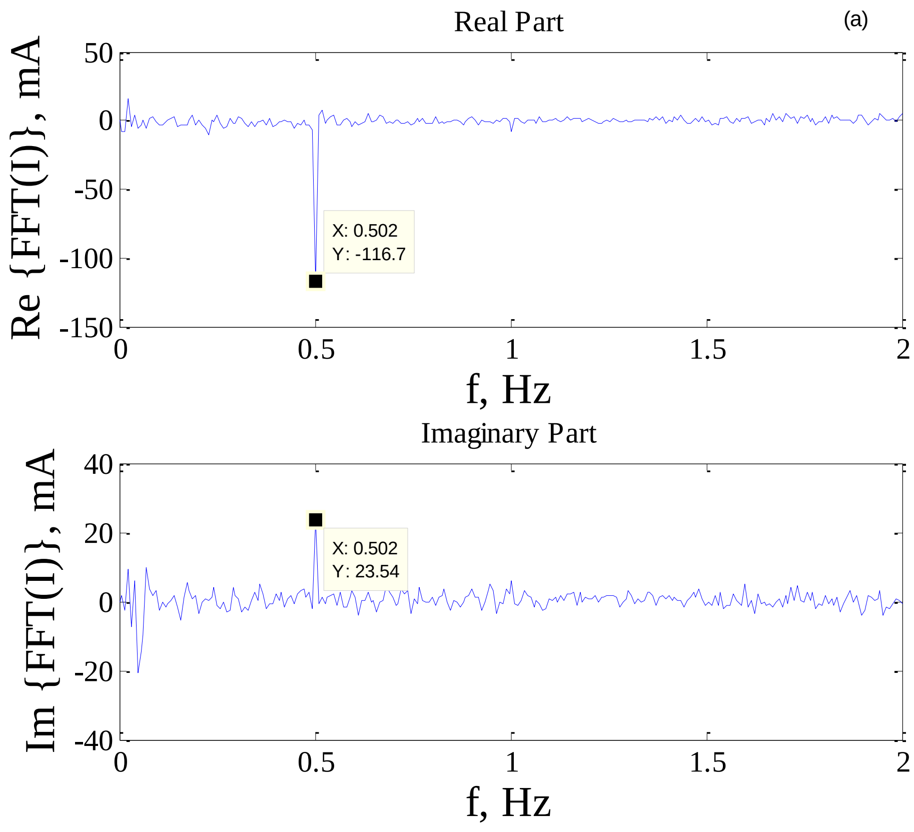

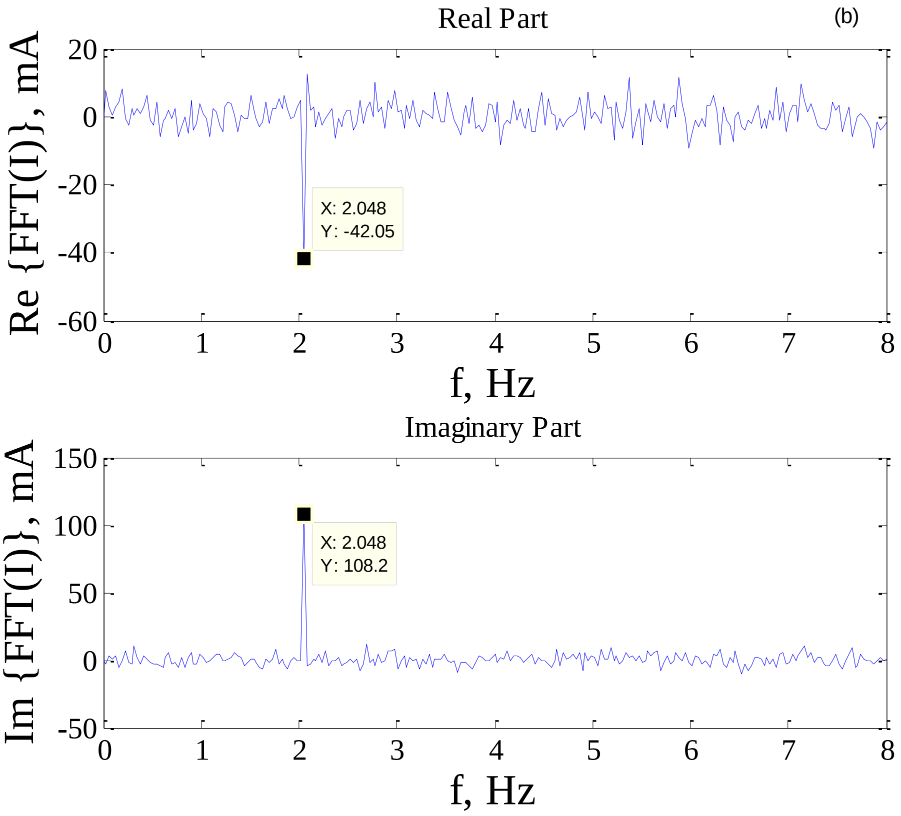

Figure 18. FFT current (a) 0.5Hz, 339mA mean current; (b) 2Hz, 487mA mean current.

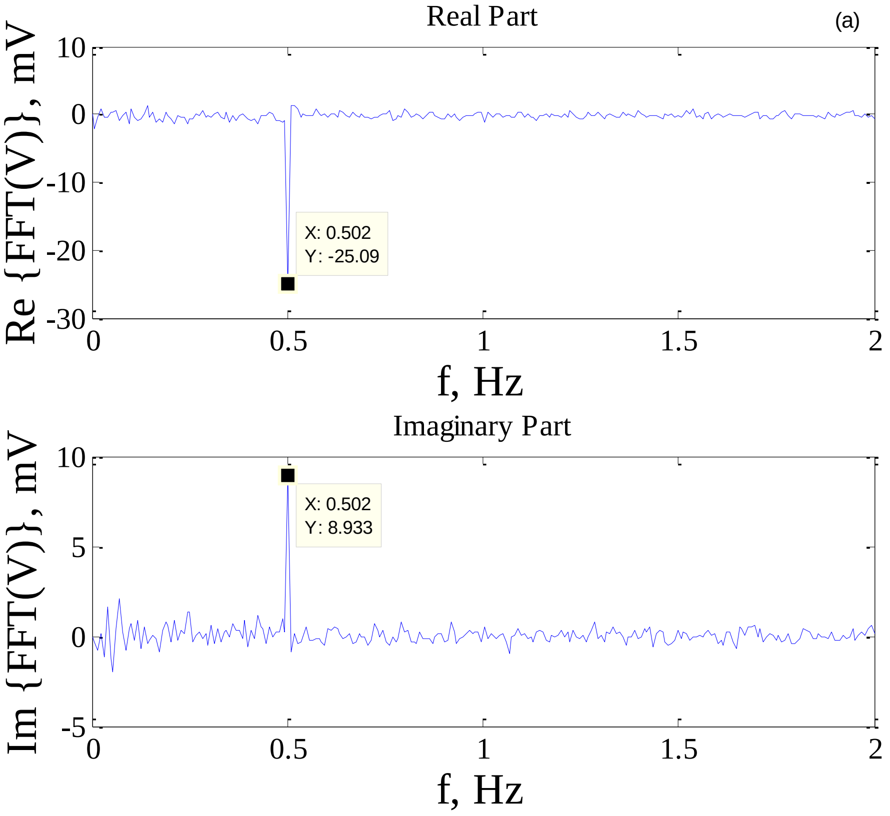

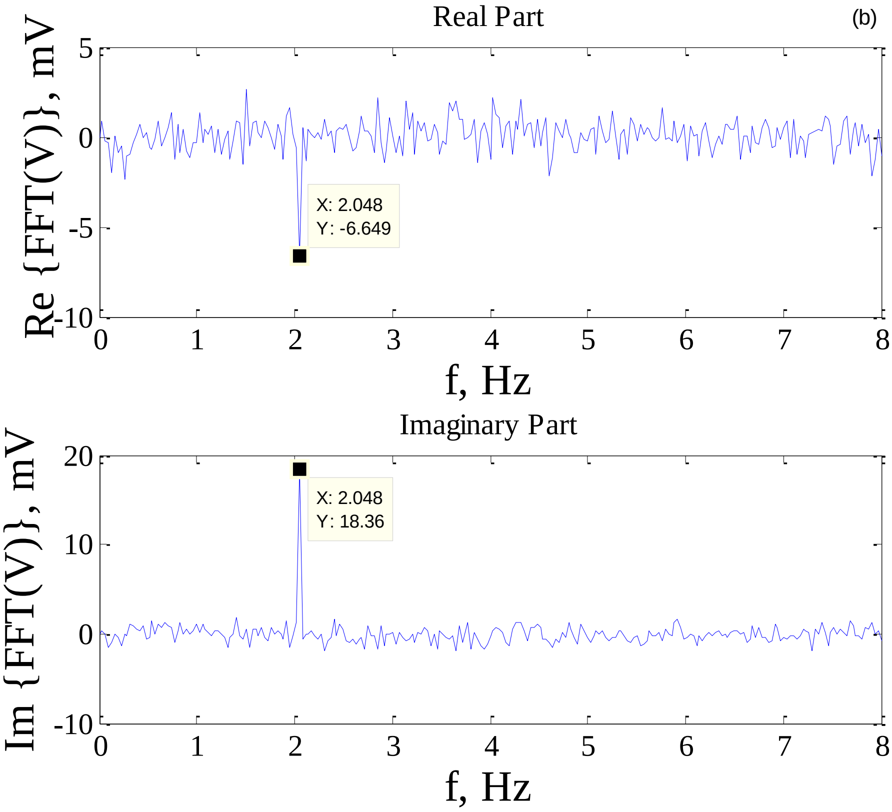

Figure 19. FFT voltage at (a) 0.5Hz, 3714mV mean voltage; (b) 2Hz, 3725mV mean voltage.

The first order harmonics in Figure 18 and Figure 19 clearly indicate the existence of current and voltage signal at 0.5Hz and 2Hz. Small errors of first harmonic location are due to inconsistent sampling time intervals mentioned above.

The real and imaginary part of the FFT results correspond to $\Delta I_{re}, \Delta V_{re}$ and ΔI_{im}, ΔV_{im} respectively. At 0.5Hz, according to equation (24).

$$\left|\frac{\Delta V_{re}}{V_0}\right| = \frac{25.09}{3714} = 0.68\% \ll \left|\frac{\Delta I_{re}}{I_0}\right| = \frac{116.7}{337} = 34.62\%$$

$$\left|\frac{\Delta V_{im}}{V_0}\right| = \frac{8.933}{3714} = 0.24\% \ll \left|\frac{\Delta I_{im}}{I_0}\right| = \frac{23.54}{337} = 6.98\%$$

At 2Hz:

$$\left|\frac{\Delta V_{re}}{V_0}\right| = 0.18\% \ll \left|\frac{\Delta I_{re}}{I_0}\right| = 8.63\%$$

$$\left|\frac{\Delta V_{im}}{V_0}\right| = 0.49\% \ll \left|\frac{\Delta I_{im}}{I_0}\right| = 22.22\%$$

The fluctuation of voltage, relative to its mean value, is much smaller than the fluctuation of current compared to its mean.

According to the analysis in section 2.4, the assumption that a power modulation gives rise to a (leading order) pseudo-current perturbation appears valid. The actual power fluctuation excited by the App can be considered a current perturbation approximately.

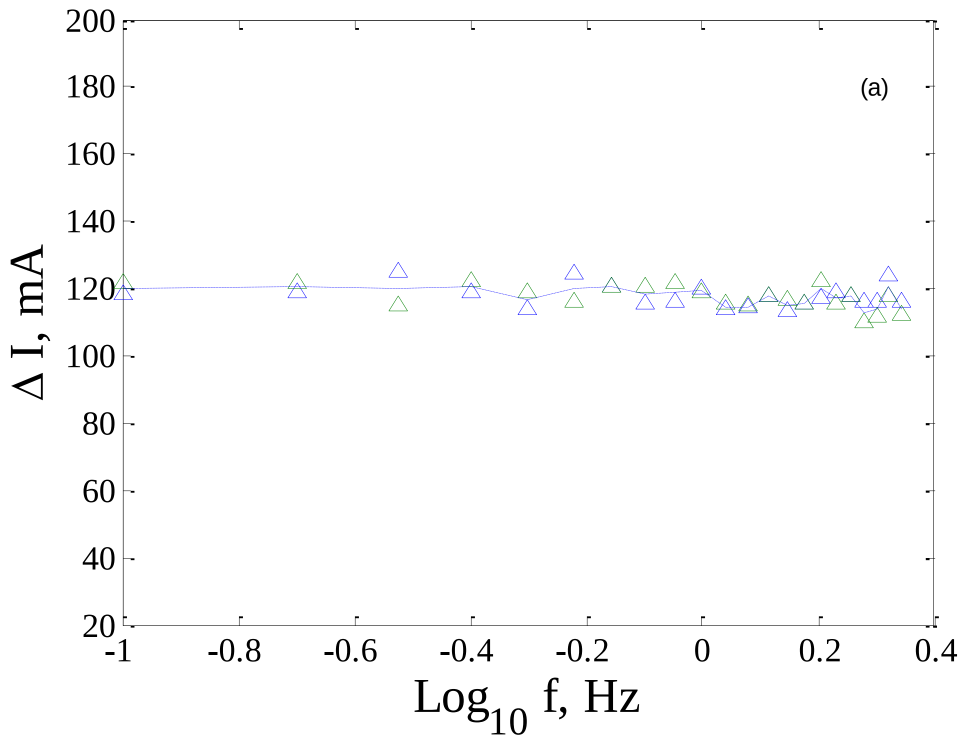

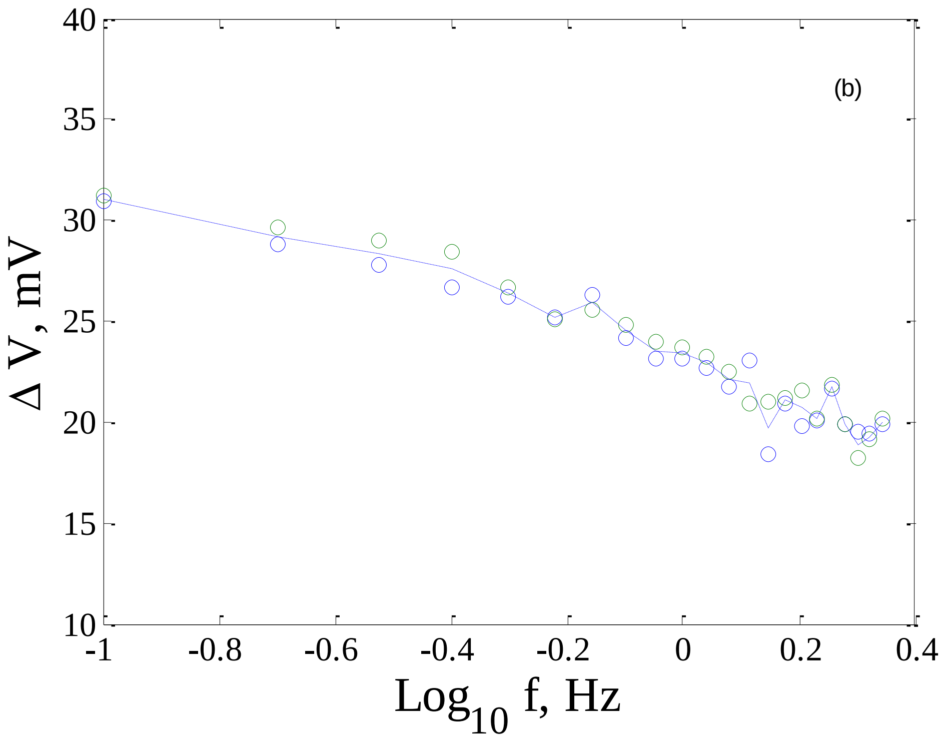

Figure 20. (a) Current amplitude spectrum and (b) voltage amplitude spectrum.

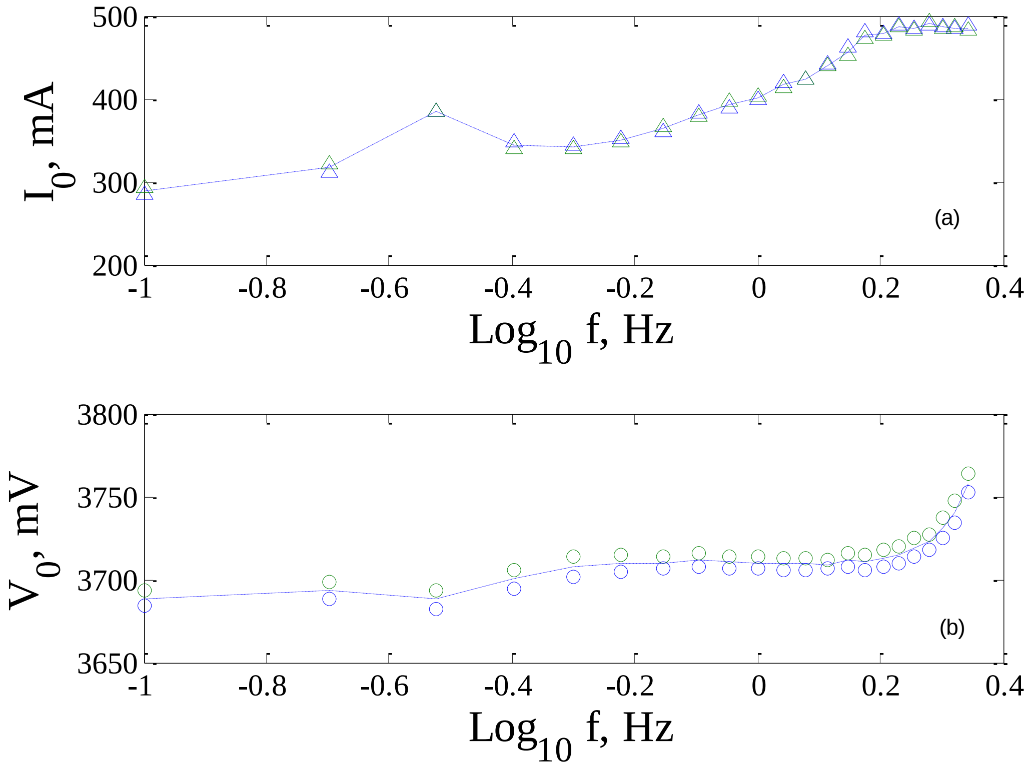

Figure 21. (a) Mean current spectrum and (b) mean voltage spectrum..

The steady current amplitudes shown in Figure 20(a) indicate the good quality of the current perturbation. The variation of voltage amplitudes shown in Figure 20(b) is due to $Z_{battery}$. The mean current drift in Figure 21(a) is expected due to the increasing usage of CPU discussed in section 4.2.2. The mean voltage drift in Figure 21(b) is due to the continuous discharging of the battery during the experiments. But voltage becomes more stable after reaching 3.7V. The possible reason is that the indication of 50% SOC of battery from the phone at 3.75V is inaccurate. The battery is still in the nonlinear region of charge/discharge curve at 3.75V, where the voltage drops fast.

Impedance of the battery can be calculated in following steps in Matlab. For signal at frequency f

$$Z_f = \frac{FFT(V)_f}{FFT(I)_f} \tag{33}$$

where, $FFT(V)_f, FFT(I)_f$ indicate the Fast Fourier Transfer result of the first harmonic located at frequency f, which are both complex numbers.

For example at 0.5Hz, from Figure 18(a) and Figure 19(a):

$$Z_{0.5} = \frac{FFT_{0.5}}{FFT(I)_{0.5}} = \frac{-25.09 + 8.933j}{-116.7 + 23.54j} = 0.221 - 0.032j$$

The impedances for different frequencies can be calculated in the same scenarios, and then assembled to form the Nyquist Plot and Bode Plot in Figure 23. Limited by the range of experimental frequencies available, the Nyquist Plot only covers the larger semicircle in the medium to low frequency range, which means the impedance of negative electrode is not observed. Hence, the ECM used for fitting is simplified as:

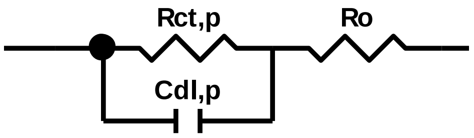

Figure 22. Simplified ECM.

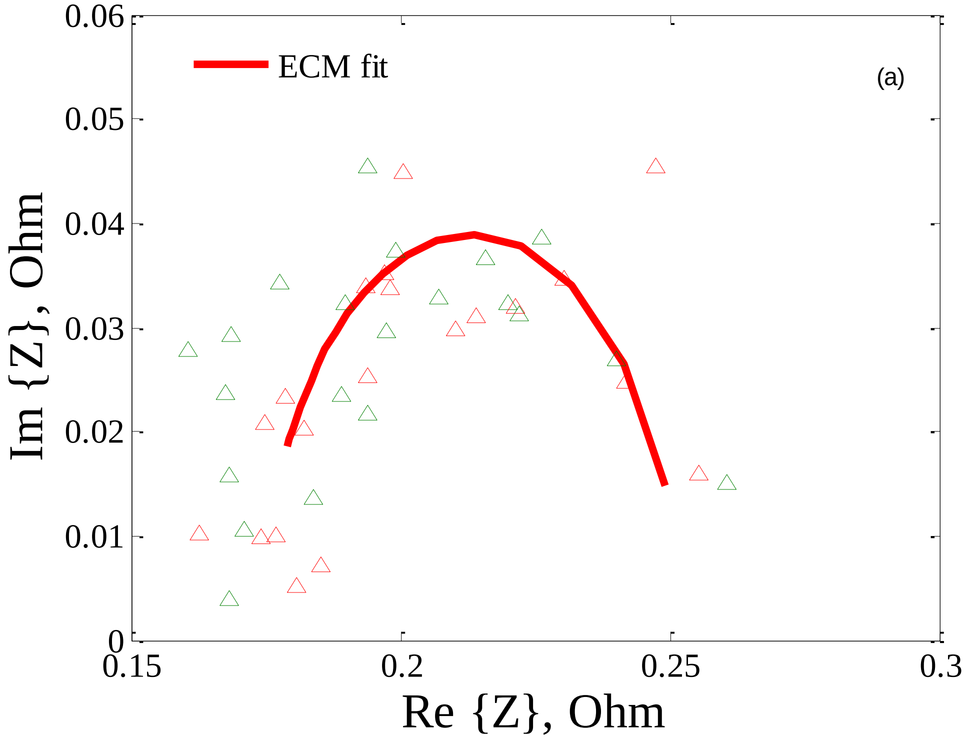

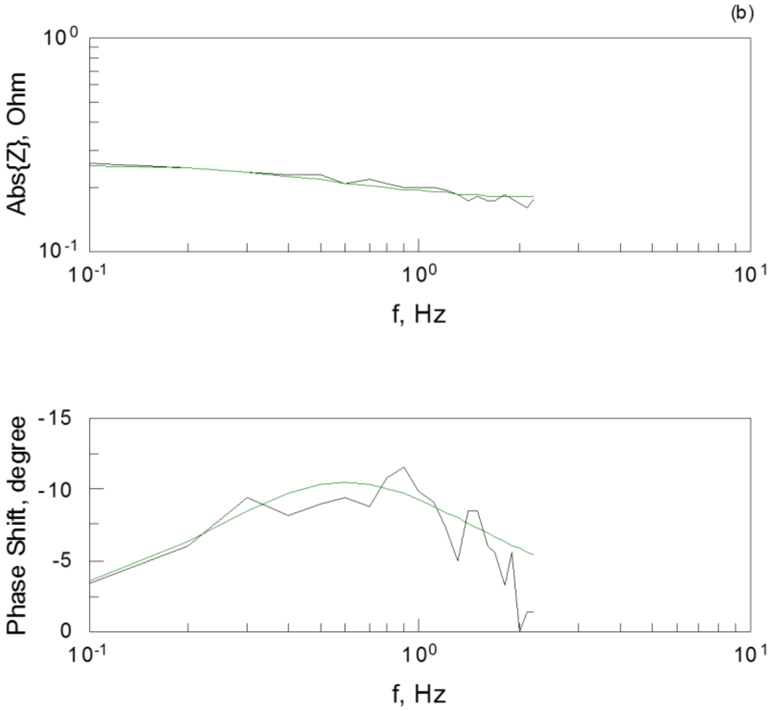

Figure 23. Impedance Spectrum of EV-30 measured by phone.(a) Nyquist plot, (b)Bode plot.

By visually inspecting in Figure 23(a), $R_0 \approx 0.15\Omega$, $\approx 0.26\Omega - 0.15\Omega = 0.11\Omega$. According to the ECM fitting, $R_0 = 0.1736\Omega$, $R_{ct,p} = 0.0777\Omega$, $C_{dl,p} = 4.14F$. Compared with the 350 mA mean current EIS results in Table 2. $R_0 = 0.16625\Omega$, $R_{ct,p} = 0.10756\Omega$, $C_{dl,p} = 1.589F$, the estimation of R_0 from the phone is consistent with standard result, but the difference between $C_{dl,p}$ is significant. $R_{ct,p}$ determined visually is closer to the standard value than the one estimated from ECM. Since the fitness of ECM at high frequency is not good in Figure 23 (b), the accuracy of $R_{ct,p}$ derived from ECM is affected.

Furthermore, the battery keeps discharging during experiments, which means the SOC of battery is theoretically different for impedance measurements at every frequency corresponding to every single point on Nyquist Plot. For example, at 0.1Hz, the mean discharging current is 300mA. Since 64 cycles of perturbation are excited for each frequency consumed charge during an experiment at 0.1Hz is $300mA * 64 * \frac{1}{0.1Hz} = 53.3mAh$, which corresponds to a 2% SOC changes compared to a total capacity of 2500mAh. Approximately, running the whole frequency spectrum on the phone once will make SOC decrease by 9-10% SOC as shown in Figure 24. Based on the discussion about the relationship between SOC and battery impedance in previous sections, the Nyqusit Plot and impedance results derived from the phone readings are the combination of impedance behaviors of battery at different mean current and SOCs. Moreover, because the battery impedance is very small, current fluctuations caused by any background processes can pollute the impedance data. In addition, the inconsistent sampling time interval affects the accuracy of Fast Fourier Transform results and introduces error into the calculation of battery impedance.

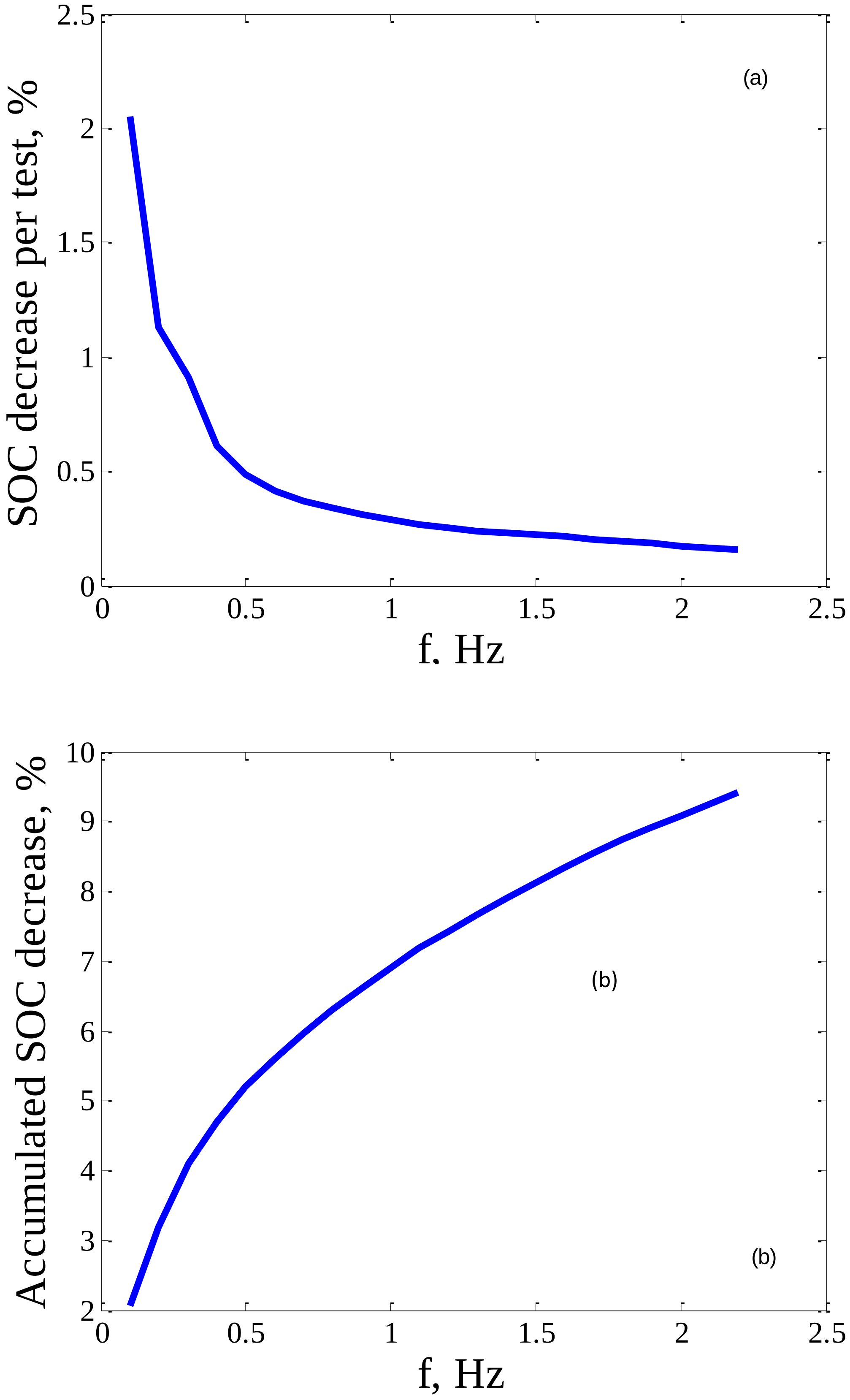

Figure 24, (a) SOC decrease for each perturbation frequency, (b) Accumulated SOC decrease.

Errors due to the background process and sampling time interval definitely can be minimized with better App programing to kill all irrelevant processes during experiments, and with more powerful CPU and chipset that can sample more precisely at the set time interval. For errors caused by SOC drift, three possible solutions are suggested:

1) Decrease the experimental time at each frequency to minimize the decrease on SOC. The sampling points per cycle should increase at the same time to maintain the quality of data.
2) Decrease the number of low frequency experiments to minimize the decrease on SOC. From Figure 24(b), it can be seen that the SOC decreases significantly after removing the 4 low frequency experiments at 0.1Hz, 0.2Hz, 0.3Hz and 0.5Hz. If the same impedance results can be obtain without these points, there is no need to do experiments at these low frequency. The ECM fitting results with decreasing number of low frequency experiments are shown in Table 3.

Frequency Range	R_o (Ω)	$R_{ct,p}$ (Ω)	SOC% decrease
0.1Hz-2.2Hz	0.17364	0.07775	9.4
0.2Hz-2.2Hz	0.17306	0.07515	7.36
0.3Hz-2.2Hz	0.17291	0.07457	6.25
0.5Hz-2.2Hz	0.17205	0.07039	4.63
0.8Hz-2.2Hz	0.17181	0.07172	3.41
1Hz-2.2Hz	0.17052	0.05886	2.8

Table 3. ECM fitting results with different frequency range.

It can be observed that the calculated results of R_o and $R_{ct,p}$ has very small variation until the lowest frequency points is set to be 1Hz. But for experiment at 0.8Hz-2.2Hz, the SOC only decreases 3.41% during the full spectrum test, which is only 1/3 of the original experiment. Hence, decreasing the number of low frequency experiments can help maintaining the SOC steady during experiments.

3) Use single point experiment at low enough frequency f_d, where the impedance is close to the sum of R_o and $R_{ct,p}$. For SOC estimation, $R_{ct,p}$ presents significant dependence on SOC but R_o is almost constant, which means the dependence of $(R_o + R_{ct,p})$ on SOC correspond to the dependence of $R_{ct,p}$. Furthermore, both R_o and $R_{ct,p}$ are related to SOH and RUL estimation. Hence, one single experiment at the specific frequency may provide enough impedance information for estimation SOC, SOH and RUL. For example, a single experiment at 0.1Hz will only cause 2.04% decrease of the SOC.

5. Conclusion

We reviewed the dependency of impedance behavior, including double-layer capacitance, charge-transfer resistance, ohmic resistance and Warburg impedance, on SOC and SOH determination in batteries. Within these impedance elements, the charge-transfer resistance is found to significantly depend on SOC and SOH. Secondly, we described how widely used methods including coulomb counting method and open circuit voltage method are not accurate. In the rest of the thesis, we introduced a new method to implement EIS on portable devices. An App is designed and prototyped on the phone as an illustration of the approach. The feasibility and reliability of the App, and quality of the data collected from the App, are validated with experimental results. By comparing the impedance data derived from the phone with the reference data, it is shown that the mobile phone has the ability to produce a modulated current at the battery by screen modulations and to then extract useful impedance information from the battery. In addition, the Android system has the ability to do complex calculation. Hence, with better App programming, more powerful CPU, faster battery monitoring chipset and advanced experimental methods, it is practical to run an EIS measurement on the phone independently and use the impedance information to identify the SOC and SOH of the phone battery. This is a potentially valuable new characterization tool for on-device battery diagnostics.

6. References

[1] T.Osaka, H.Nara, D. Mukoyama, T. Yokoshima. New Analysis of Electrochemical Impedance Spectroscopy for Lithium-ion batteries. J. Electrochem. Soc, 157-162,(2013).

[2] W. Y. Chang, “State of charge estimation for LiFePO4 battery, using artificial neural network,” International Review of Electrical, Engineering, vol. 7, no. 5, pp. 5874–5800, 2012.

[3] Klein, R.; Chaturvedi, N.A.; Christensen, J.; Ahmed, J.; Findeisen, R.; Kojic, A., "Electrochemical Model Based Observer Design for a Lithium-Ion Battery," Control Systems Technology, IEEE Transactions on, vol.21, no.2, pp.289,301, March 2013

[4] Z. H. Rao, S. F. Wang, and G. Q. Zhang, “Simulation and experiment of thermal energy management with phase change material for ageing LiFePO4 power battery,” Energy Conversion and Management, vol. 52, no. 12, pp. 3408–3414, 2011.

[5] Wen-Yeau Chang, “The State of Charge Estimating Methods for Battery: A Review,” ISRN Applied Mathematics, vol. 2013, Article ID 953792, 7 pages, 2013.

[6] M. Becker, G. Traufetter. Boeing Wählte Brandgefährliches Batteriematerial, (21.03.2013) Der Spiegel Online,

URL:http://www.spiegel.de.offcampus.lib.washington.edu/wissenschaft/technik/dreamliner-akkus-boeing-waehlte-brandgefaehrliches-batteriematerial-a-878759.html

[7] Chaturvedi, N.A.; Klein, R.; Christensen, J.; Ahmed, J.; Kojic, A., "Algorithms for Advanced Battery-Management Systems," Control Systems, IEEE , vol.30, no.3, pp.49,68, June 2010

[8] N. A. Chaturvedi , R. Klein , J. Christensen , J. Ahmed and A. Kojic "Modeling, estimation, and control challenges for lithium-ion batteries", Proc. Amer. Control Conf. (ACC), pp.1997 -2002 2010

[9] Sabine Piller, Marion Perrin, Andreas Jossen, Methods for state-of-charge determination and their applications, Journal of Power Sources, Volume 96, Issue 1, 1 June 2001, Pages 113-120, ISSN 0378-7753

[10] A. A. A. Elgammal and A. M. Sharaf, “Self-regulating particle swarm optimised controller for (photovoltaic-fuel cell) battery charging of hybrid electric vehicles,” IET Electrical Systems in Transportation, vol. 2, no. 2, pp. 77–89, 2012.

[11] Jun Huang, Jianbo Zhang,Zhe Li,Shaoling Song,Ningning Wu, “Exloring Differences between Charge and Discharge of LiMn2O4/Li Half-Cell with Dynamic Electrochemical Impedance Spectroscopy”,Electrochimica Acta 131,(2014) 228-235.

[12] Technote 31: Electrochemical Impedance Spectroscopy (EIS) for Battery Research and Development, http://www.solartronanalytical.com/Literature/Technical-Notes.aspx

[13] W. Waag, S. Kabitz, D.U. Sauer Experimental investigation of the lithium-ion battery impedance characteristic at various conditions and aging states and its influence on the application J. Applied Energy, 102 (2013), pp. 885–897

[14] Jingliang Zhang, Jay Lee, A review on prognostics and health monitoring of Li-ion battery, Journal of Power Sources, Volume 196, Issue 15, 1 August 2011, Pages 6007-6014, ISSN 0378-7753

[15] H.Nara, S. Tominaka, T. Momma, and T. Osaka, J. Electrochem. Soc,158,158,B1184 (2011)

[16] H.Nara, T. Momma, and T. Osaka, Electrochimica Acta, 113,720 (2013)

[17] Basics of Electrochemical Impedance Spectroscopy, Gamry Instruments, http://www.gamry.com/application-notes/EIS/basics-of-electrochemical-impedance-spectroscopy/

[18] Yuanyuan Xie, Jianyang Li, Chris Yuan, Mathematical modeling of the electrochemical impedance spectroscopy in lithium ion battery cycling, Electrochimica Acta, Volume 127, 1 May 2014, Pages 266-275, ISSN 0013-4686

[19] F. Huet, A review of impedance measurements for determination of the state-of-charge or state-of-health of secondary batteries, Journal of Power Sources, Volume 70, Issue 1, 30 January 1998, Pages 59-69, ISSN 0378-7753

[20] M.E. Orazem, B. Tribollet, Electrochemical impedance spectroscopy, (first ed.) John Wiley & Sons, New Jersey (2008)

[21] R.S. Robinson, System noise as a signal source for impedance measurements on batteries connected to operating equipment, Journal of Power Sources, Volume 42, Issue 3, 8 February 1993, Pages 381-388, ISSN 0378-7753

[22] Robinson, R.S., "System noise as a signal source for impedance measurements on battery strings," Telecommunications Energy Conference, INTELEC '93. 15th International , vol.2, no., pp.365,368 vol.2, 27-30 Sep 1993

[23] M. Hughes, R.T. Barton, S.A.G.R. Karunathilaka, N.A. Hampson, R. Leek, The impedance of 23 Ah Ni-Cd cells with sintered electrodes: measurements in the range 10 kHz-0.001 Hz as an indication of residual capacity. J. Appl. Electrochem., 15 (1985), pp. 129–137

[24] S.A.G.R. Karunathilaka, R.T. Barton, M. Hughes, N.A. Hampson. Faradaic impedance measurements of small magnitudes encountered in high capacity electrical storage cells. J. Appl. Electrochem., 15 (1985), pp. 251–257

[25] Jamie Gomez, Ruben Nelson, Egwu E. Kalu, Mark H. Weatherspoon, Jim P. Zheng, Equivalent circuit model parameters of a high-power Li-ion battery: Thermal and state of charge effects, Journal of Power Sources, Volume 196, Issue 10, 15 May 2011, Pages

4826-4831, ISSN 0378-7753

[26] P. Mauracher, E. Karden, Dynamic modelling of lead/acid batteries using impedance spectroscopy for parameter identification, Journal of Power Sources, Volume 67, Issues 1–2, July–August 1997, Pages 69-84, ISSN 0378-7753

[27] Christian Fleischer, Wladislaw Waag, Hans-Martin Heyn, Dirk Uwe Sauer, On-line adaptive battery impedance parameter and state estimation considering physical principles in reduced order equivalent circuit battery models: Part 1. Requirements, critical review of methods and modeling, Journal of Power Sources, Volume 260, 15 August 2014, Pages 276-291, ISSN 0378-7753

[28] S. Buller. Impedance Based Simulation Models for Energy Storage Devices in Advanced Automotive Power Systems. (Ph.D. thesis) RWTH Aachen University (2003)

[29] P. Mauracher, E. Karden, Dynamic modelling of lead/acid batteries using impedance spectroscopy for parameter identification, Journal of Power Sources, Volume 67, Issues 1–2, July–August 1997, Pages 69-84, ISSN 0378-7753

[30] Shalini Rodrigues, N. Munichandraiah, A.K. Shukla, A review of state-of-charge indication of batteries by means of a.c. impedance measurements, Journal of Power Sources, Volume 87, Issues 1–2, April 2000, Pages 12-20, ISSN 0378-7753

[31] Hampson, N.A., Karunathilaka, S.A.G.R., Leek, R. The impedance of electrical storage cells(1980) Journal of Applied Electrochemistry, 10 (1), pp. 3-11

[32] Masayuki Itagaki, Keiichirou Honda, Yoshinao Hoshi, Isao Shitanda, In-situ EIS to determine impedance spectra of lithium-ion rechargeable batteries during charge and discharge cycle, Journal of Electroanalytical Chemistry, Volume 737, 15 January 2015, Pages 78-84, ISSN 1572-6657

[33] Jun Huang, Jianbo Zhang, Zhe Li, Shaoling Song, Ningning Wu, Exploring Differences between Charge and Discharge of LiMn2O4/Li Half-cell with Dynamic Electrochemical Impedance Spectroscopy, Electrochimica Acta, Volume 131, 10 June 2014, Pages 228-235, ISSN 0013-4686

[34]Alvin J Salkind, Craig Fennie, Pritpal Singh, Terrill Atwater, David E Reisner, Determination of state-of-charge and state-of-health of batteries by fuzzy logic methodology, Journal of Power Sources, Volume 80, Issues 1–2, July 1999, Pages 293-300, ISSN 0378-7753

[35] Akram Eddahech, Olivier Briat, Nicolas Bertrand, Jean-Yves Delétage, Jean-Michel Vinassa, Behavior and state-of-health monitoring of Li-ion batteries using impedance spectroscopy and recurrent neural networks, International Journal of Electrical Power & Energy Systems, Volume 42, Issue 1, November 2012, Pages 487-494, ISSN 0142-0615

[36] Holger Blanke, Oliver Bohlen, Stephan Buller, Rik W. De Doncker, Birger Fricke,

Abderrezak Hammouche, Dirk Linzen, Marc Thele, Dirk Uwe Sauer, Impedance measurements on lead–acid batteries for state-of-charge, state-of-health and cranking capability prognosis in electric and hybrid electric vehicles, Journal of Power Sources, Volume 144, Issue 2, 15 June 2005, Pages 418-425, ISSN 0378-7753

[37] Jamie Gomez, Ruben Nelson, Egwu E. Kalu, Mark H. Weatherspoon, Jim P. Zheng, Equivalent circuit model parameters of a high-power Li-ion battery: Thermal and state of charge effects, Journal of Power Sources, Volume 196, Issue 10, 15 May 2011, Pages 4826-4831, ISSN 0378-7753

[38] Wladislaw Waag, Stefan Käbitz, Dirk Uwe Sauer, Experimental investigation of the lithium-ion battery impedance characteristic at various conditions and aging states and its influence on the application, Applied Energy, Volume 102, February 2013, Pages 885-897, ISSN 0306-2619

[39] Christian Fleischer, Wladislaw Waag, Hans-Martin Heyn, Dirk Uwe Sauer, On-line adaptive battery impedance parameter and state estimation considering physical principles in reduced order equivalent circuit battery models part 2. Parameter and state estimation, Journal of Power Sources, Volume 262, 15 September 2014, Pages 457-482, ISSN 0378-7753

[40] Alexander Bartlett, James Marcicki, Kevin Rhodes, Giorgio Rizzoni, State of health estimation in composite electrode lithium-ion cells, Journal of Power Sources, Volume 284, 15 June 2015, Pages 642-649, ISSN 0378-7753

[41] Saha, B., Goebel, K., Poll, S., & Christophersen, J. (2007). A Bayesian framework for remaining useful life estimation. In Proceedings Fall AAAI symposium: AI for prognostics. Arlington.

[42] P. Arora, R. White, Capacity fade mechanisms and side reactions in lithium-ion batteries, J. Electrochem. Soc., 145 (10) (1998), pp. 3647–3667

[43] J. Vetter, P. Novák, M.R. Wagner, C. Veit, K.-C. Möller, J.O. Besenhard, M. Winter, M. Wohlfahrt-Mehrens, C. Vogler, A. Hammouche, Ageing mechanisms in lithium-ion batteries, Journal of Power Sources, Volume 147, Issues 1–2, 9 September 2005, Pages 269-281, ISSN 0378-7753

[44] P. Barai, P. Mukherjee, Stochastic analysis of diffusion induced damage in lithium-ion battery electrodes, J. Electrochem. Soc., 160 (6) (2013), pp. A955–A967

[45] G. L. Plett, “Extended Kalman filtering for battery management systems of LiPB-based HEV battery packs: Part 3. State and parameter estimation,” J. Power Sources, vol. 134, no. 2, pp. 277–292, Aug. 2004

[46] K. Smith, “Electrochemical control of lithium-ion batteries [applications of control],” IEEE Control Syst. Mag., vol. 30, no. 2, pp. 18–25, Apr. 2010.

[47] S. Santhanagopalan and R. E. White, “Online estimation of the state of charge of a

lithium ion cell," J. Power Sources, vol. 161, no. 2, pp. 1346–1355, 2006.

[48] Tom Saxton, Chief Science Officer, Tesla Roadster Battery Study, Released: July 13, 2013, http://www.pluginamerica.org/surveys/batteries/tesla-roadster/PIA-Roadster-Battery-Study.pdf

[49] M. Coleman, C. K. Lee, C. Zhu, and W. G. Hurley, "State of charge determination from EMF voltage estimation: using impedance, terminal voltage, and current for lead-acid and lithium-ion batteries," IEEE Transactions on Industrial Electronics, vol. 54, no. 5, pp. 2550–2557, 2007.

[50] T. Dong, J. Li, F. Zhao et al., "Analysis on the influence of measurement error on state of charge estimation of LiFePO4power battery," in Proceedings of the International Conference on Materials for Renewable Energy and Environment (ICMREE '11), pp. 644–649, Shanghai, China, May 2011.

[51] S. Lee, J. Kim, J. Lee, and B. H. Cho, "State-of-charge and capacity estimation of lithium-ion battery using a new open circuit voltage versus state-of-charge," Journal of Power Sources, vol. 185, no. 2, pp. 1367–1373, 2008

[52] K. S. Ng, C. S. Moo, Y. P. Chen, and Y. C. Hsieh, "Enhanced Coulomb counting method for estimating state-of-charge and state-of-health of lithium-ion batteries," Applied Energy, vol. 86, no. 9, pp. 1506–1511, 2009.

[53] Carat, By University of Helsinkhttps://itunes.apple.com/us/app/carat/id504771500

[54] http://batteryscore.com/help/

[55] http://www.maximintegrated.com/en/products/power/battery-management/DS2438.html